N73-32059
NASA CR-2317

NASA CONTRACTOR REPORT

NASA CR-2317



# A PARAMETRIC STUDY OF CUT-OFF CORRUGATED SURFACE PROPERTIES

*by C. A. Mentzer and L. Peters, Jr.*

*Prepared by*
OHIO STATE UNIVERSITY
Columbus, Ohio 43212
*for Langley Research Center*

NATIONAL AERONAUTICS AND SPACE ADMINISTRATION • WASHINGTON, D. C. • OCTOBER 1973

| 1 Report No | 2 Government Accession No | 3. Recipient's Catalog No |
|---|---|---|
| NASA CR-2317 | | |

| 4 Title and Subtitle | 5 Report Date |
|---|---|
| A PARAMETRIC STUDY OF CUT-OFF CORRUGATED SURFACE PROPERTIES | October 1973 |
| | 6 Performing Organization Code |

| 7 Author(s) | 8 Performing Organization Report No |
|---|---|
| C. A. Mentzer and L. Peters, Jr. | |
| | 10 Work Unit No |
| 9 Performing Organization Name and Address | 630-52-00-01 |
| Ohio State University | 11 Contract or Grant No |
| Columbus, Ohio 43212 | NAS1-10040 |
| | 13 Type of Report and Period Covered |
| 12 Sponsoring Agency Name and Address | Contractor Report |
| National Aeronautics and Space Administration<br>Washington, D.C. 20546 | 14 Sponsoring Agency Code |

15 Supplementary Notes

This is a topical report.

16 Abstract

*Corrugated horns involve a junction between the corrugated surface and a conducting* groundplane. Proper horn design requires an understanding of the electromagnetic properties of the corrugated surface and this junction. Therefore, an integral equation solution has been used to study the influence of corrugation density and shape on the power loss. Surface current, and the scattering from a groundplane-corrugated surface junction Both square and vee shape corrugations have been considered over the range of corrugation depths where the surface acts as a cut-off corrugated surface.

| 17 Key Words (Suggested by Author(s)) | 18 Distribution Statement |
|---|---|
| Radiometric Antennas<br>Corrugated Surfaces | Unclassified - Unlimited |

| 19 Security Classif (of this report) | 20 Security Classif (of this page) | 21 No of Pages | 22 Price* |
|---|---|---|---|
| Unclassified | Unclassified | 59 | Domestic, $3.50<br>Foreign, $6.00 |

*For sale by the National Technical Information Service, Springfield, Virginia 22151

TABLE OF CONTENTS

## I. INTRODUCTION

The corrugated horn has been established as an antenna with low side and back lobes, rotationally symmetric patterns (for square pyramidal and conical horn shapes), and broad-band performance[1-8]. These properties make this horn useful for many applications; including the one presently under study, i.e., as a radiometer antenna. A ray optics model of the dominant radiation mechanisms of conventional horn antennas is shown in Fig. 1a. In the corrugated horn (shown in profile

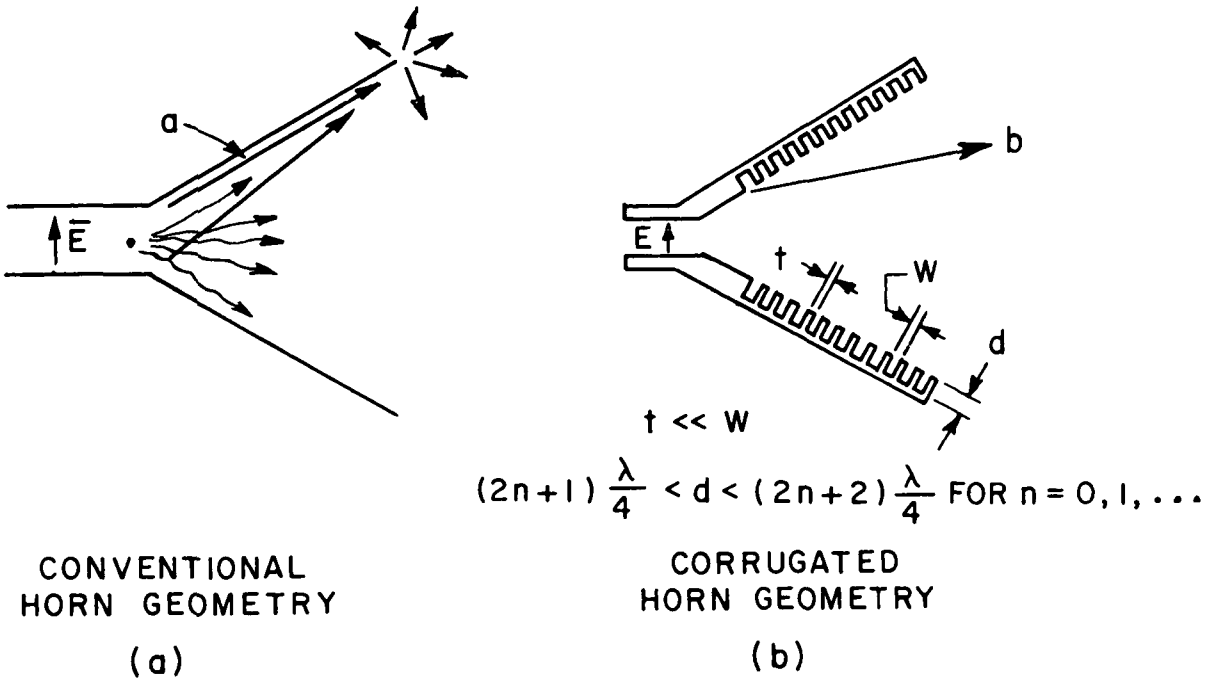


Fig. 1. a) Conventional horn geometry b) Corrugated horn geometry

in Fig. 1b) the corrugated surface (with capacitive surface impedance in the E-plane of the horn) serves to reduce or eliminate the fields associated with ray "a" of Fig. 1a. This in turn reduces or eliminates the usual high E-plane sidelobes. The influence of the corrugation shape and density on the scattering from the onset of the corrugations and on the losses in the horn has been ignored in previous work. The parametric study reported here attempts to generate further understanding of the operating

principles of the corrugated horn and to establish design criteria for the construction of practical corrugated horn geometries through a detailed analysis of the groundplane corrugated surface junction. The analysis includes studying the surface currents flowing on the corrugations and the loss in the corrugations as well as the scattering from the onset of the corrugations. The usual corrugated horn requirements are for 8 or more corrugations per wavelength and a corrugation depth "d" between $0.25\lambda$ and $0.5\lambda$.* In addition, it is usually specified that the tooth thickness ("t" in Fig. 1b) should be much less than the corrugation width ("W" in Fig.1b). In order to study the effects of varying these parameters, an integral equation solution was used to find the radiated fields and the surface currents associated with the groundplane corrugated surface models of Fig. 2. A brief description of the integral formulation is included in the next section and the results are presented in the following section.

The groundplane-corrugated surface models shown in Fig. 2 were chosen for their similarity to one wall of a sectoral corrugated horn. In the corrugated horn, the illumination of the corrugations is by a cylindrical wave due to the diffraction from the horn-waveguide junction In the model used, the magnetic line source pair provides a similar cylindrical wave illumination while at the same time allows placing a null in the far field in the direction of the adjacent edge of the groundplane. Then one need not match over the entire groundplane but only over the illuminated part, thus saving the limited number of match points for the corrugated surface side of the model. The remaining match points are divided among the 20 corrugations. For all corrugation depths where cut-off operation is obtained (i.e., $0.25 \leq d/\lambda < 0.5$ for the square corrugation), the energy is forced away from the corrugated surface. Since the energy is forced off the corrugations, the corrugated surface matching points may be terminated without affecting the currents in the corrugations near the junction. Thus the surface model need not be closed. This conclusion was verified by finding the currents and scattered fields associated with the open model shown and a similar closed model and observing no significant differences. Therefore, this finite model is a good approximation to an infinite groundplane corrugated surface junction as long as the corrugated surface is operated in the cut-off mode.

---

*This depth would be in free space wavelengths for the parallel plate waveguide geometry of the corrugations. If the sides of the slot are terminated in a conducting plane, then these electrical lengths would correspond to those of the $TE_{10}$ waveguide mode. Thus, some improvement in the operating bandwidth of the pyramidal corrugated horn could be achieved if the depth of the first few corrugations are appropriately tapered.

## II. METHOD OF SOLUTION

The surface currents on the corrugations and the scattering by the groundplane-corrugated surface junction of Fig. 2 were found using the H-field formulation for the transverse electric field case discussed by Harrington[9]. For this case, there is only a z component of magnetic field, $H$, and a tangential component of surface current, $\bar{J}$($\bar{J} = n \times \bar{H}$, where $n$ is the unit normal). At any point, the total magnetic field, $H_z$, is the sum of the incident and scattered magnetic fields, $H_z^i$ and $H_z^s$ respectively. The scattered field is related to its source, the surface current, by

$$(1) \qquad H_z^s = \hat{U}_z \cdot \bar{\nabla} \times \int JG \, d\bar{\ell}'$$

where $\bar{J} = J \, d\bar{\ell}' = -[H_z]_{C^+} d\bar{\ell}'$ when $H_z$ is evaluated on $C^+$ (just outside the contour C where the surface current, $\bar{J}$, flows - the interior of C lies on the left side of $d\bar{\ell}'$).

and G is the two-dimensional Green's function $G(\bar{\rho},\bar{\rho}') = 1/4jH_0^{(2)}k(|\bar{\rho}-\bar{\rho}'|)$. The resulting integral equation

$$(2) \qquad J = -[H_z^i + \hat{U}_z \cdot \bar{\nabla} \times \int JG \, d\bar{\ell}']_{C^+}$$

is solved for the surface current, J, by point matching using pulse basis functions. This integral equation reduces to the matrix equation

$$(3) \qquad [\ell_{mn}] \, [f_n] = [g_m]$$

where $[\ell_{mn}] = j/4k \, \Delta C_n \, (\hat{n} \cdot \bar{R}) H_1^{(2)}(k|\bar{\rho}_m - \bar{\rho}_n|)$

= matrix of coupling coefficients between the $m^{th}$ and the $n^{th}$ segments at $\rho_m$ and $\rho_n$ on the surface contour.

$\bar{R} = \dfrac{\bar{\rho}_m - \bar{\rho}_n}{|\bar{\rho}_m - \bar{\rho}_n|}$ = unit vector between $n^{th}$ and $m^{th}$ points,

$\Delta C_n = J_n \, d\bar{\ell}$ = current moment at the $n^{th}$ point,

$[f_n]$ = column vector of unknown surface current on $n^{th}$ segment at the points $(x_n,y_n)$ on the surface contour,

and $[g_m]$ = column vector of incident field ($= -H_z^i$) at the points $(X_m,Y_m)$ on the surface contour.

This matrix equation has veen solved for the surfaces shown in Fig. 2 using a Crout[10] matrix inversion subroutine. Other more powerful inversion

subroutines which included pivoting and iterative improvement were used for comparison but provided no improvement beyond the 3 to 5 place accuracy obtained from Crout's method. These other methods were not used regularly because they required nearly twice the storage since both the matrix and its inverse had to be stored. The subroutine listing for the Crout method is included in Appendix A along with the rest of the computer program.

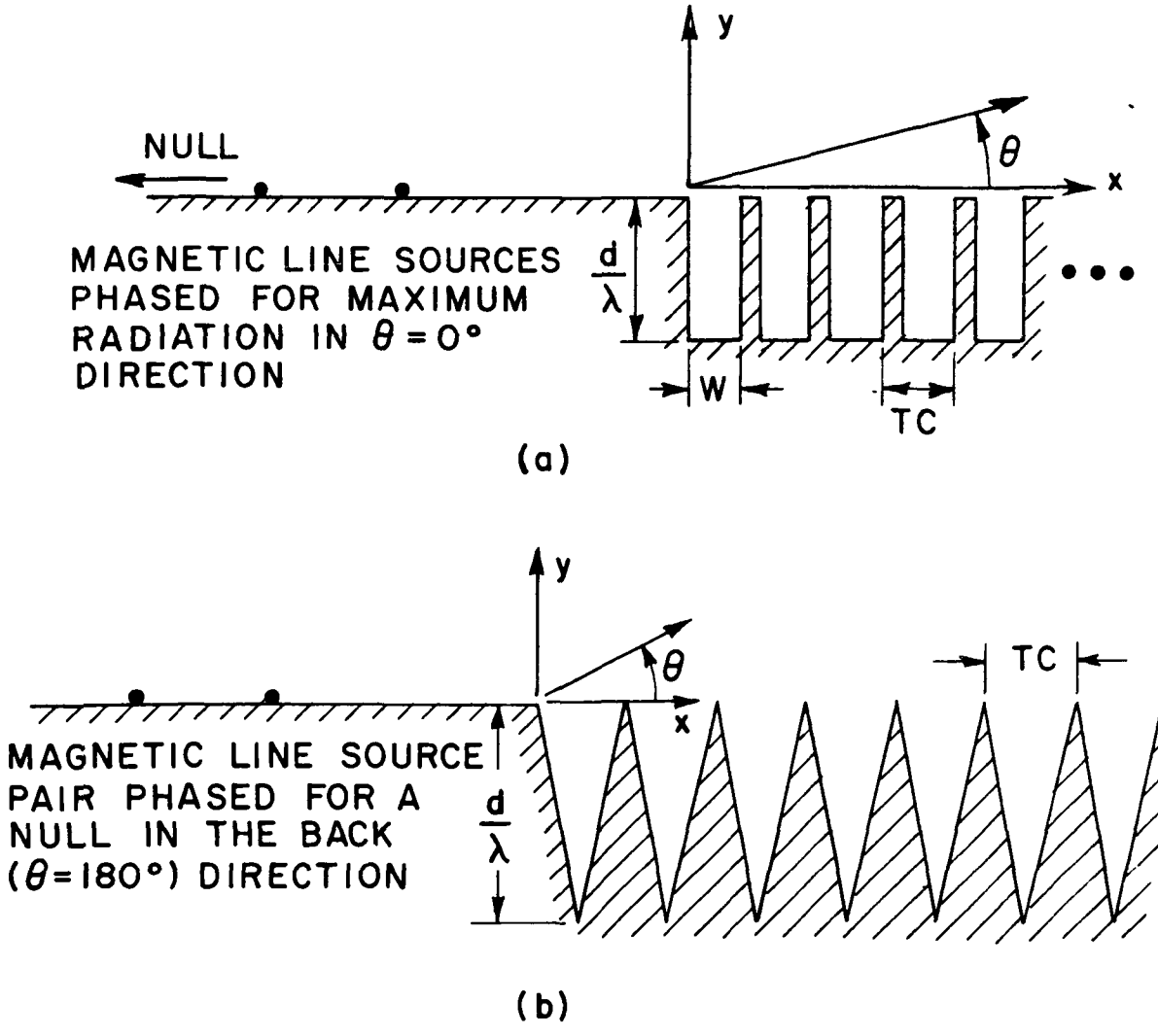


Fig. 2. Surface model used to find the scattered fields and surface currents associated with a groundplane-corrugated surface junction.

## III. RESULTS FOR SQUARE CORRUGATIONS

The parameters of the square corrugations of Fig. 2a which were varied in this study include the corrugation depth, the corrugation density and the corrugation shape. The notation used to relate these parameters to the model and the range of values considered for these parameters are shown in Table 1.

TABLE I

PARAMETERS CONSIDERED IN STUDY OF SQUARE CORRUGATIONS

| PARAMETER | NOTATION in Fig. 2a | VALUES CONSIDERED |
|---|---|---|
| Corrugation depth(in wavelengths) | $d/\lambda$ | 0.25, 0.3125, 0.375, 0.4375, 0.5 |
| Corrugation density(in corrugations per wavelength) | NCOR = 1/TC or $N/\lambda$ | 4, 6, 8, 10, 12 |
| Corrugation shape(ratio of corrugation gap width to corrugation period) | W/TC | 0.5, 0.6, 0.7, 0.75, 0.8, 0.9 |

Many combinations of these parameters were studied to ascertain the influence of each on properties such as the scattering from the groundplane-corrugated surface junction, the surface current flowing on the corrugations and also the power loss in the corrugations.

Because of computer storage limitations, only 200 matching points could be used for each surface. These points were divided to allow for at least 8 matching points per wavelength along the surface. This matching point density is adequate if the fields in the corrugations are primarily those of the TEM mode. The verification of the dominant status of the TEM mode in the corrugations is contained in the higher order mode study included in Appendix B of this report.

Of the 200 matching points available, ten were used on the groundplane side of the model of Fig. 2a. The locations of these points are indicated in Fig. 3a. The physical optics current on an infinite groundplane is shown in amplitude and phase in parts b and c of Fig. 3. Also shown in Figs. 3b and 3c by the dashed lines are the amplitude and phase of the surface

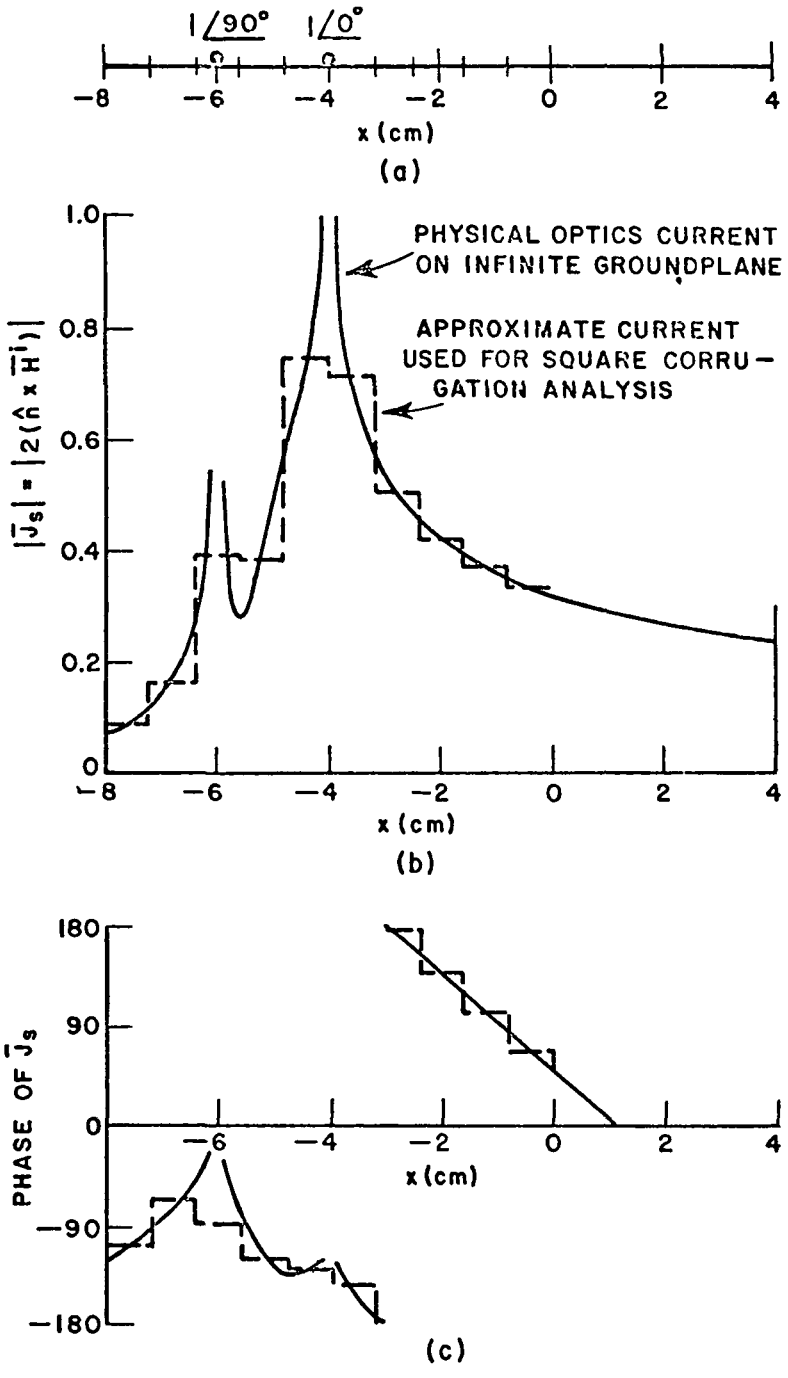


Fig. 3. Surface currents near the line sources used to model the groundplane-corrugated surface junction.
a) matching points on the groundplane side, b) surface current magnitude, c) surface current phase.

current which exists at the midpoints of the surface segments of Fig. 3a. This demonstrates that the current model used in the calculations is an accurate model of the true surface current.

The fields associated with the groundplane-corrugated surface junction are shown in Fig. 4 for corrugation depths from $0.25\lambda$ to $0.4375\lambda$. The results shown are for a corrugation density of 8 corrugations per wavelength (i.e., corrugation period = TC = $\lambda/8$) and for a corrugation shape ratio (ratio of corrugation gap width to corrugation period) of W/TC = 0.75. The patterns shown in Figs. 4a and 4b are the radiation zone total and scattered magnetic field patterns produced by the magnetic line sources of amplitude $1/z_0$ and the corrugations. The scattered field phase is shown in Fig. 4c. Notice that the direction of maximum radiation intensity varies from about $65^0$ above the corrugated surface for the $0.25\lambda$ depth to about $35^0$ for the $0.4375\lambda$ depth. All of the other corrugation densities and corrugation profiles showed essentially the same patterns at the same corrugation depths and are therefore not included. The smoothly varying phase pattern indicates that the phase center of the scattered field is nearly at the origin of the coordinate system (the junction between the groundplane and the corrugations).

This range of angles for this scattered field maximum explains the peculiar behavior of the small corrugated horn discussed previously[1]. This horn had a pattern which showed a slight frequency dependence. However, as the end of this horn was cut-off, the pattern of the remaining corrugated horn became quite frequency dependent. The geometry is shown in Fig. 1b. For the original corrugated horn, the scattered field maximum illuminated the opposite wall of the horn and weakly illuminated the aperture edge (the aperture edge was at about $43^0$). However, after the modification, the edge of the horn occurred at an angle of $50^0$ and thus was more strongly illuminated. The fields diffracted by this edge phased destructively and constructively as a function of frequency with the desired radiated field and thus caused the frequency dependent patterns. The magnetic field intensity associated with the rays diffracted by the corrugated surface junction may be expressed in the form

$$H^D = H^i \frac{e^{-jkr}}{r} F(\theta) \tag{5}$$

where $H^i$ is the magnetic field incident on the junction,
$r$ is the range as measured from the junction,
$\theta$ is the angle shown in Fig. 2, and
$F(\theta)$ is the complex pattern factor shown in Figs. 4b and 4c.

It is noted that the phase is a slowly varying function of $\theta$ and thus presents no difficulty for the application of GTD. This information is now

sufficient to compute the diffracted fields associated with ray "b" of Fig. 1b. The far field of the ray in the direction of the horn edge is readily obtained from the preceding equation. Next the surface discontinuity is replaced by a line current whose fields have that magnitude. This line current then illuminates the 90° corner at the end of the horn wall and the diffracted fields are now computed using the techniques of the Geometrical Theory of Diffraction. If the fields in the deep shadow are to be computed, then the diffraction from the thick wall is computed by representing it as a pair of 90°wedges[11]. While these computations have not been carried to completion at this time, they represent a straightforward implementation of accepted GTD practices and will yield accurate results. The major goal at this time is to establish the condition for which this edge diffraction is negligible and this would occur when the angle to the opposite edge is less than 20°-25°.

As mentioned earlier, another property of the corrugated surface which is of interest is the rate of decay of the surface current flowing on the corrugation walls. The decay in the amplitude of the surface current is due to the energy being forced away from the corrugations and not caused by power loss in the conductor. The loss will be diccussed later. Figure 5 shows the normalized surface current versus corrugation number for a surface with 8 corrugations per wavelength and a profile ratio of W/TC = 0.75 at several corrugation depths. The surface current plotted is the current which exists at the bottom of each of the 20 corrugations (point "B" in the insert) normalized with respect to the surface current which exists at the same X-coordinate on an infinite groundplane with the same sources acting (point "A" in the insert). This normalization removes the range dependence of the incident cylindrical fields and also selects the maximum current which exists on the surface of the corrugations.

Since to a good approximation only a TEM mode exists in the corrugation, the currents on the teeth at any point are given by

$$(6) \qquad |J_y| = J_s \cos\beta(d + y)$$

where y assumes negative values and $\beta = 2\pi/\lambda_o$ is the propagation constant of a TEM wave in the parallel plate waveguide region. This has also been established by all of the computations that have been made.

Notice that the most rapid decay is obtained for the $0.25\lambda$ case and as expected no decay occurs for the $0.5\lambda$ case. The variations of the current near the end of the surface are caused by fields reflected from the termination of the structure and may be ignored. This property (the decay of the surface current) has been examined for other corrugation densities and profiles. Figures 6 and 7 show the surface currents (normalized as above) existing on $0.25\lambda$ and $0.375\lambda$ deep corrugations for various corrugation densities.

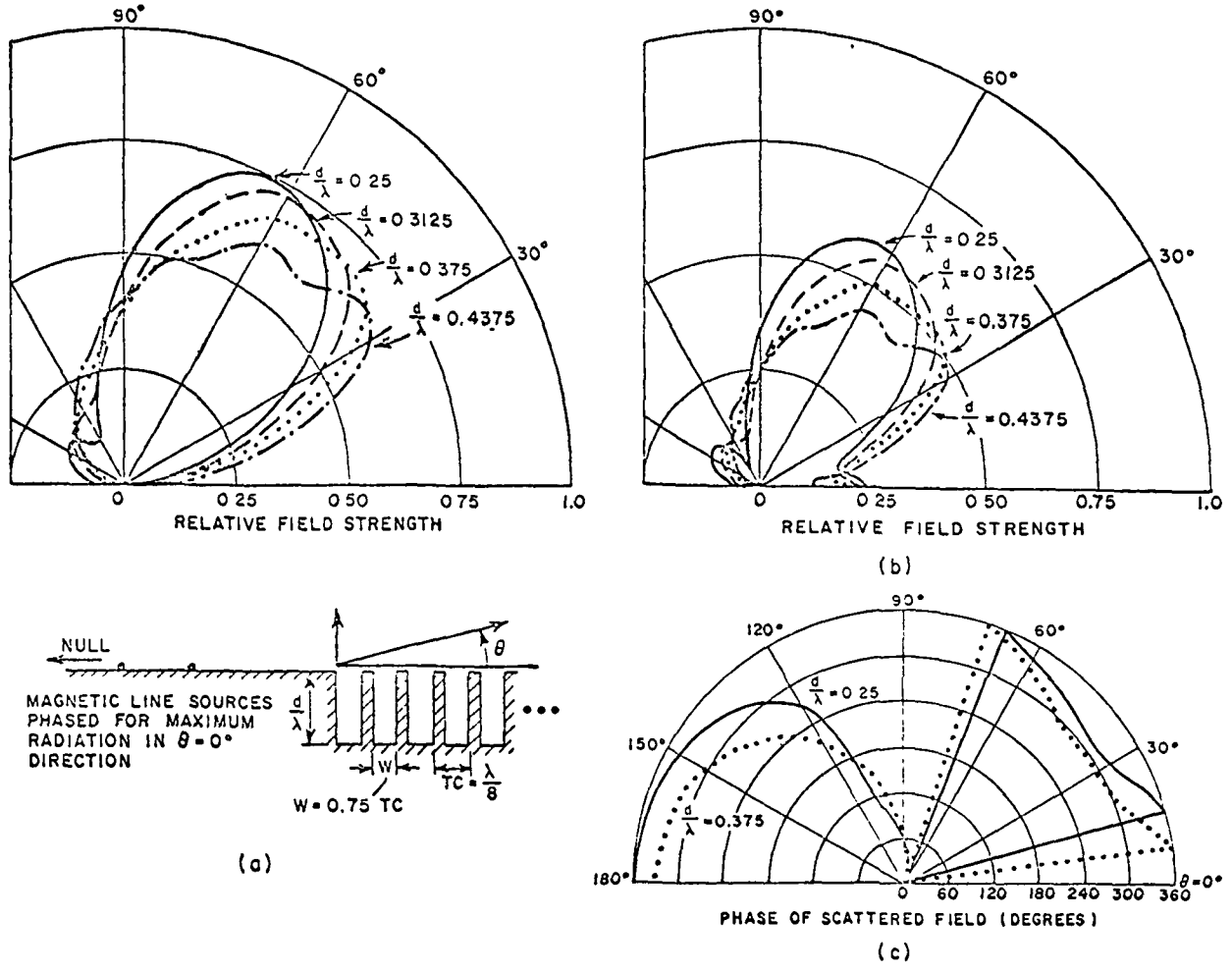


Fig. 4. Radiation pattern associated with a groundplane-corrugated surface junction illuminated by a cylindrical wave: a) total fields, b) scattered field amplitude, and c) scattered field phase

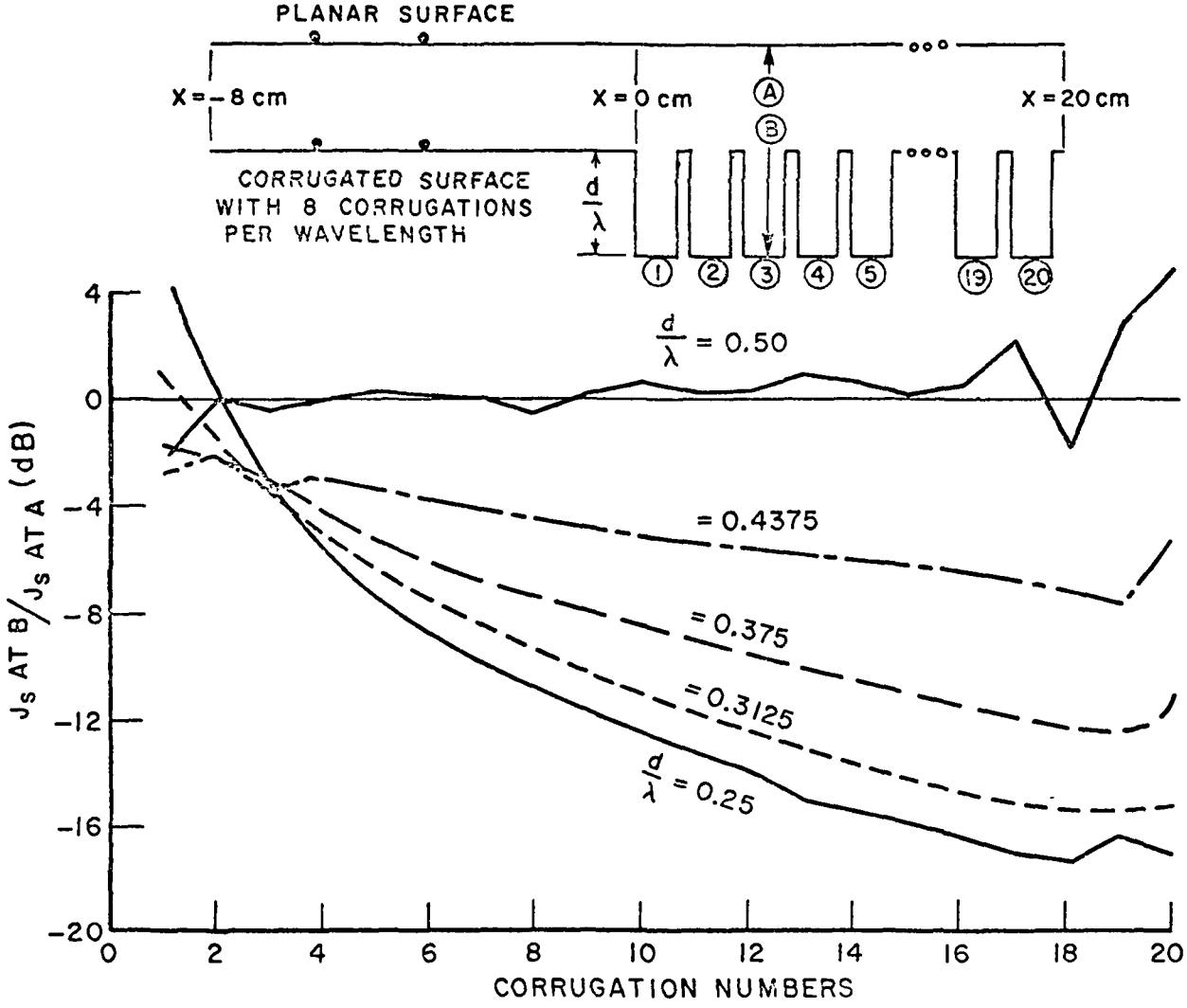


Fig. 5. Decay of surface current on a corrugated surface due to the energy being forced away from the corrugations.

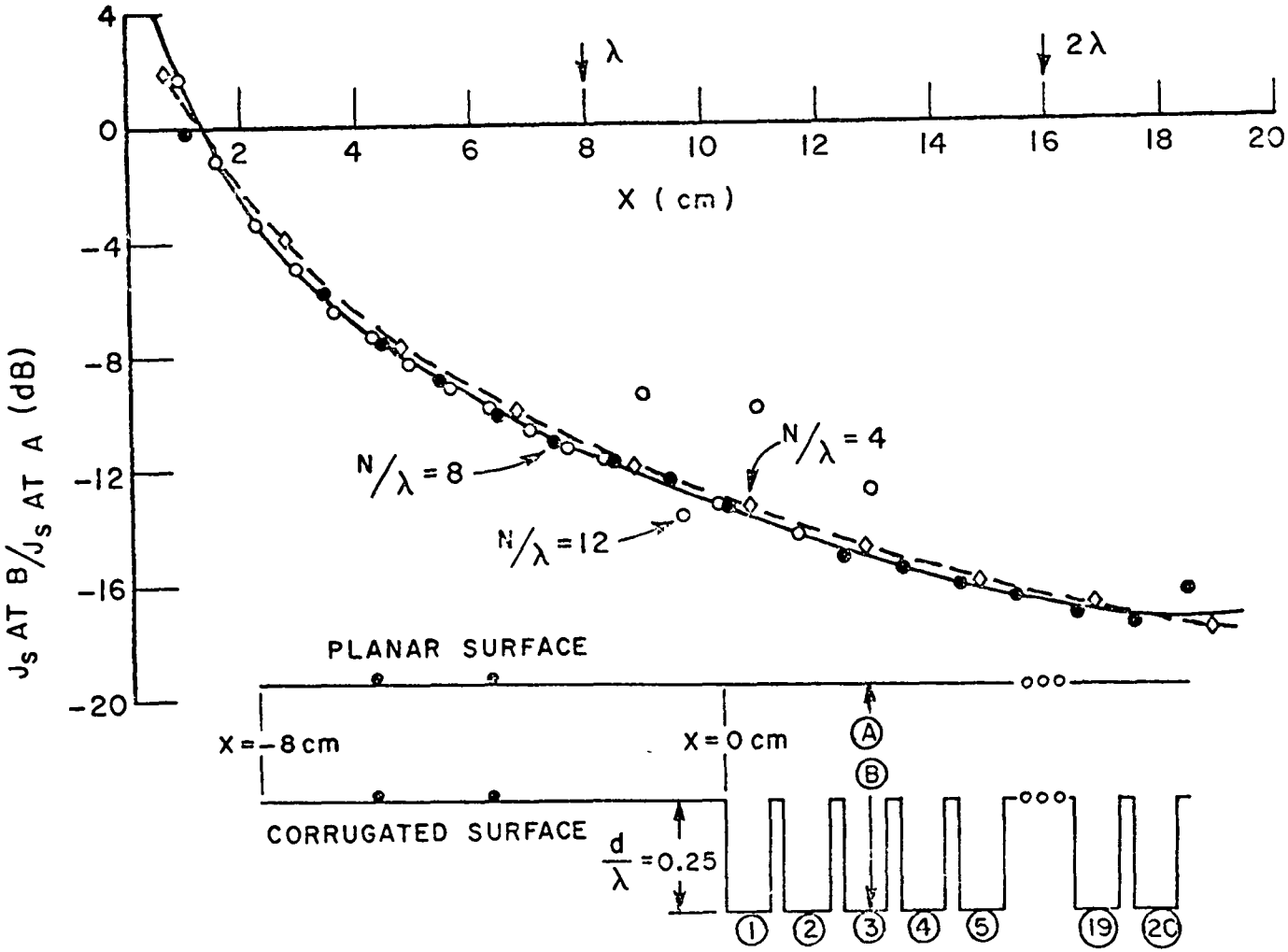


Fig. 6. Decay of surface currents on 0.25λ deep corrugations as a function of corrugation density.

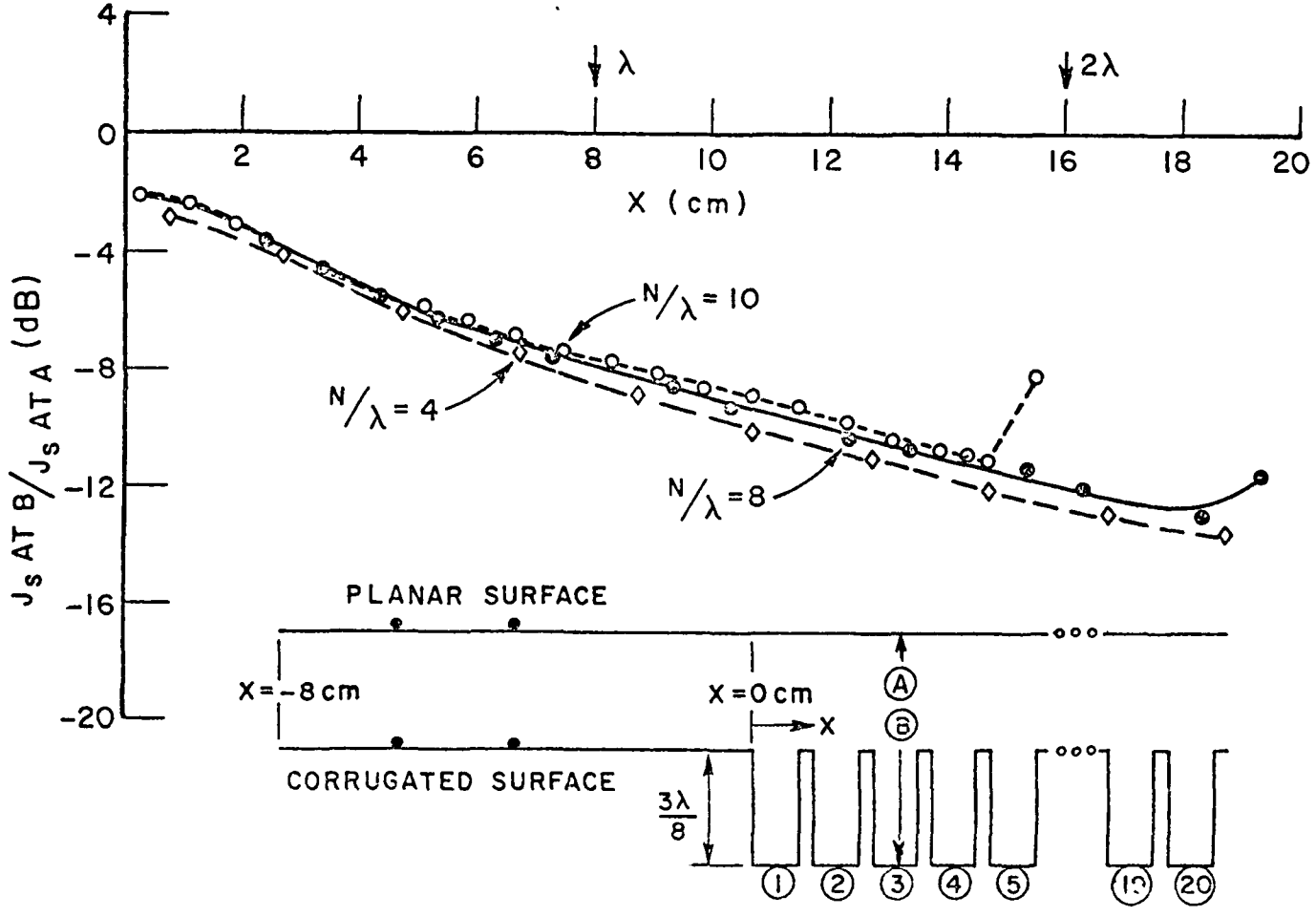


Fig. 7. Decay of surface currents on 0.375λ deep corrugations as a function of corrugation density.

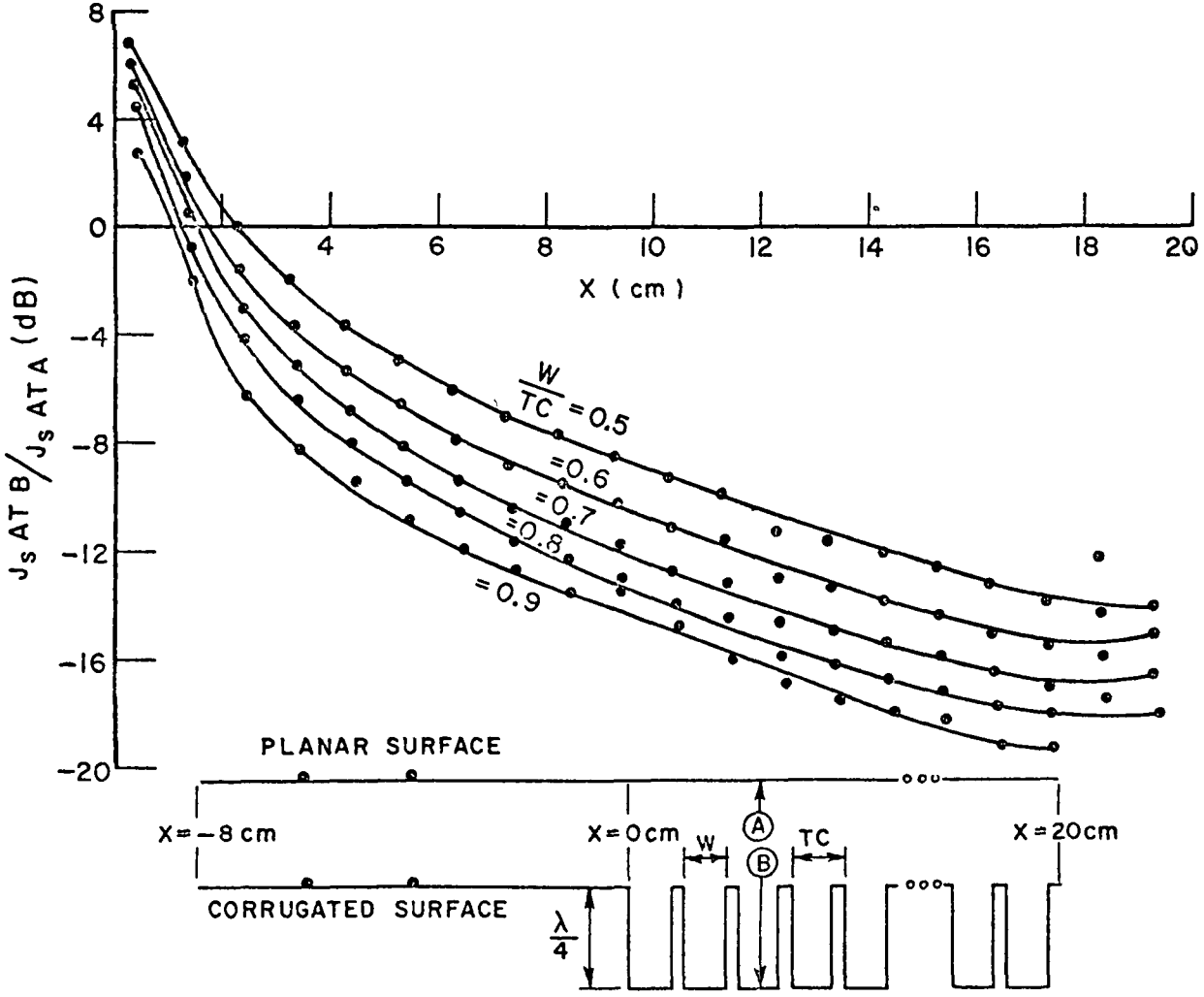


Fig. 8. Decay of surface currents on 0.25λ deep corrugations as a function of corrugation shape.

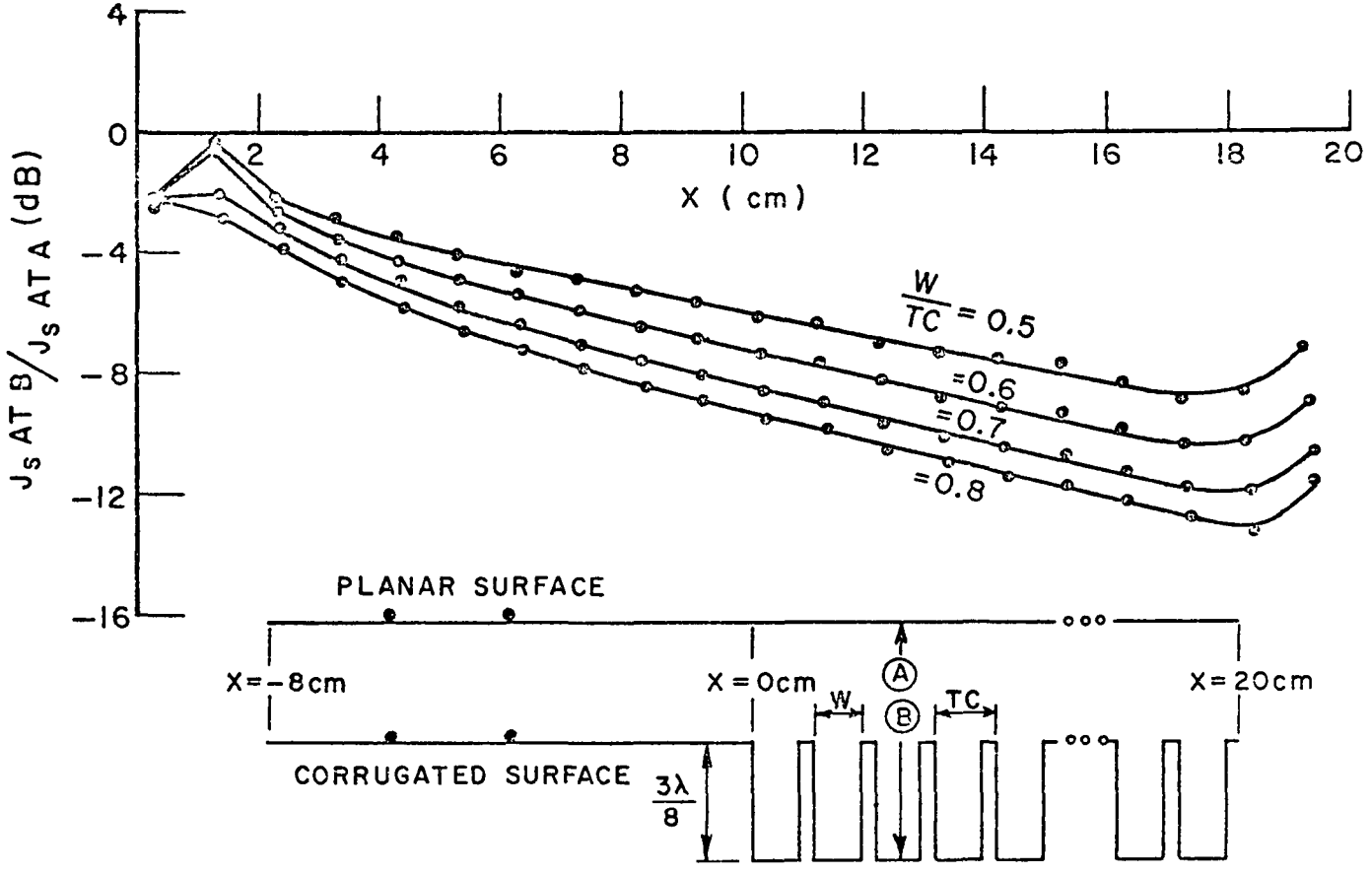


Fig. 9. Decay of surface currents on 0.375λ deep corrugations as a function of corrugation shape.

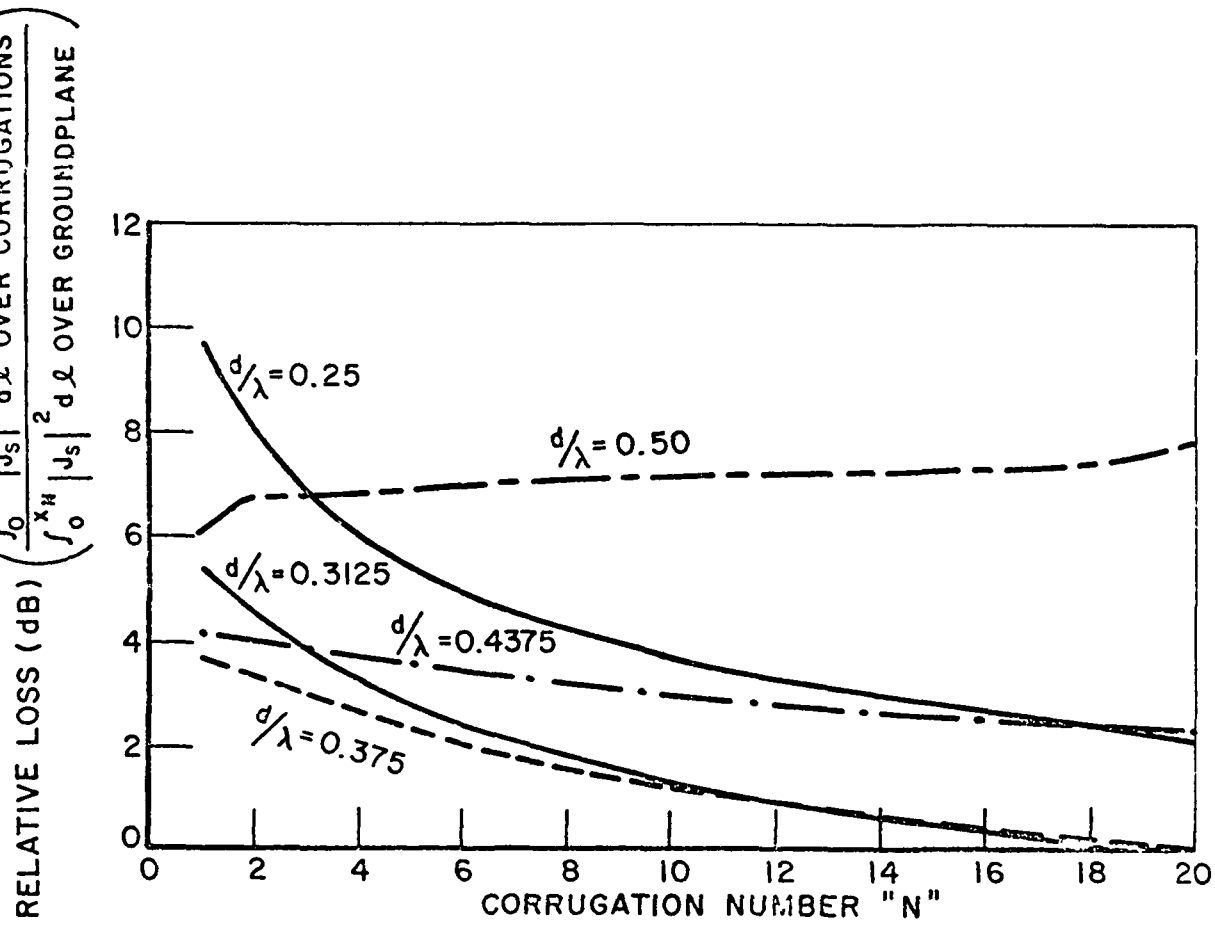


Fig. 10. Power loss in a corrugated surface for various corrugation depths.

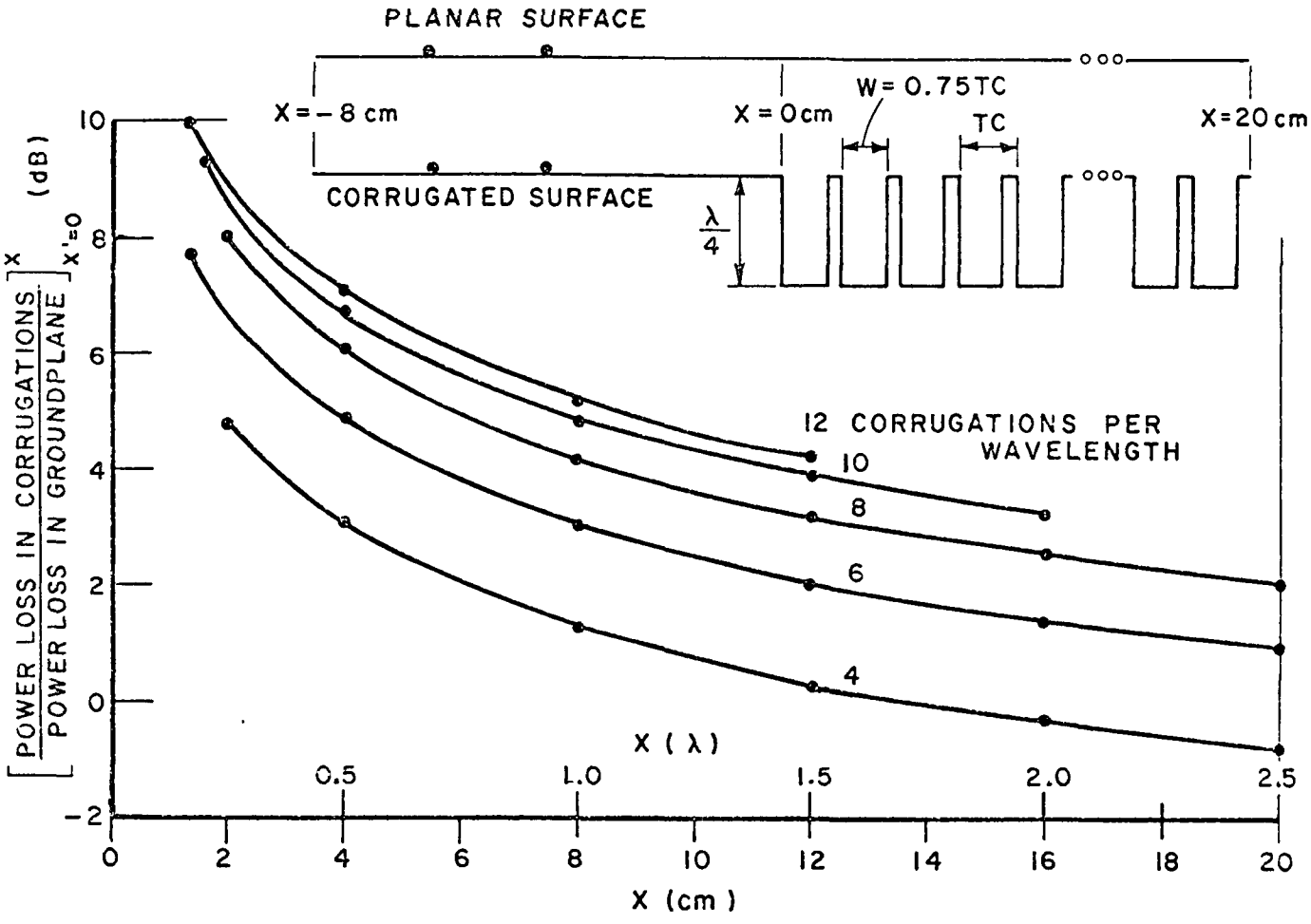


Fig. 11. Power loss in 0.25λ deep corrugations from the origin to "X" (normalized with respect to the loss in a finite segment of an infinite groundplane from the origin to "x") for various corrugation densities.

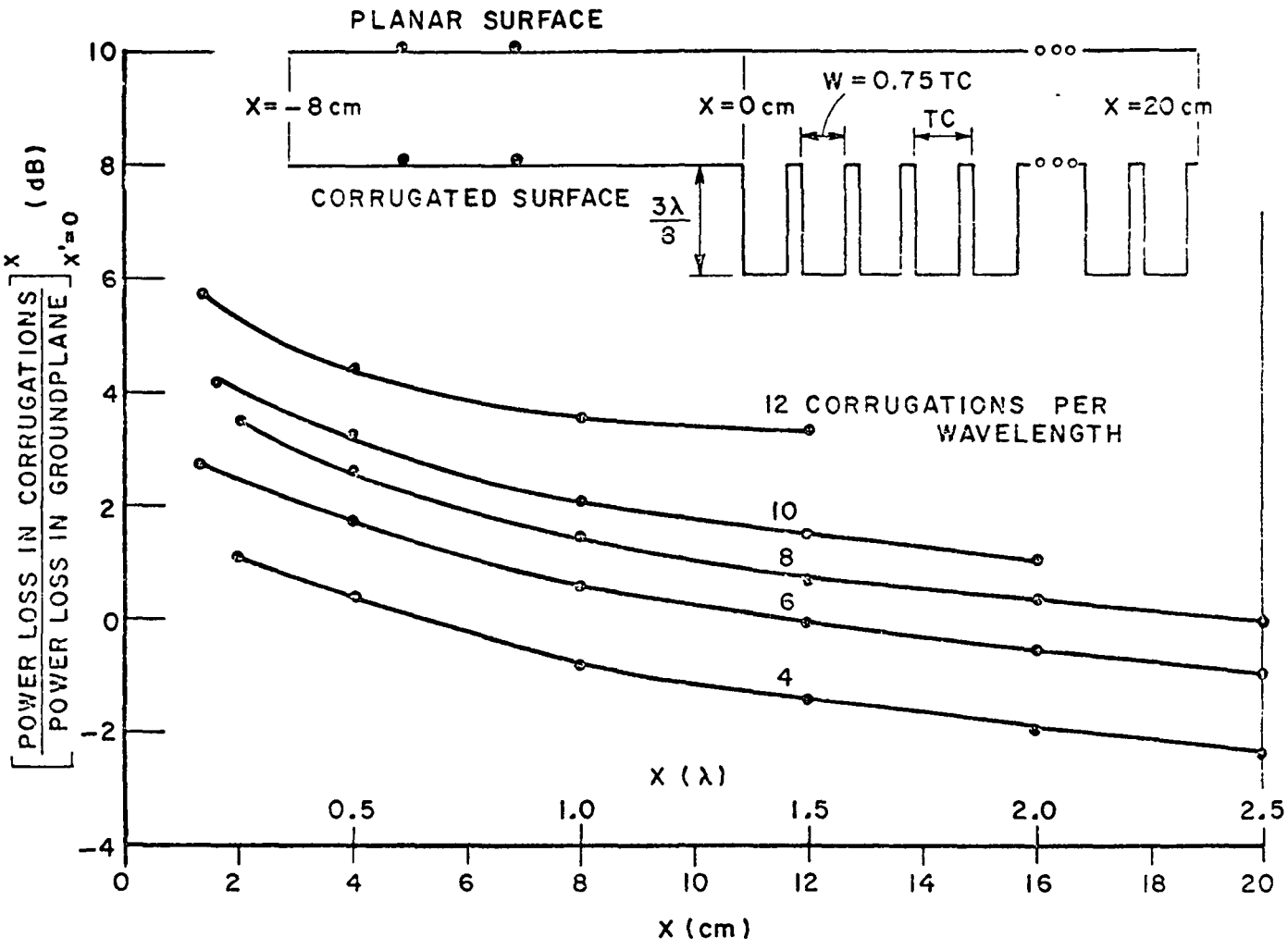


Fig. 12. Power loss in 0.375λ deep corrugations from the origin to "X" (normalized with respect to the loss in a finite segment of an infinte groundplane from the origin to "x") for various corrugation densities.

These results are plotted as a function of the X-coordinate measured in "cm" from the onset of the corrugations (the $\lambda$ and $2\lambda$ points are also shown on this scale, $\lambda$ = 8 cm). Corrugation densities ranged from 4 to 12 corrugations per wavelength and the results for each corrugation depth showed essentially no dependence on the corrugation density. The dependence of the surface current on the corrugation profile was also investigated. The corrugation profile was specified by the ratio of the corrugation gap width (W) to the corrugation period (TC) and the corrugation density was 8 corrugations per wavelength. The results are shown in Figs. 8 and 9 for $0.25\lambda$ and $0.375\lambda$ deep corrugations, respectively. The range of W/TC ratios considered was from 0.5 (thick metal vane between corrugations) to 0.9 (very thin metal vane). Beyond approximately $1/2\lambda$ from the onset of the corrugations (i.e., $x > 4$ cm for the $\lambda$ = 8 cm case shown), the decay of the surface current per wavelength is nearly constant ($\sim$ 6 dB/$\lambda$ at $d/\lambda = 0.25$ and $\sim$ 4 dB/$\lambda$ at $d/\lambda = 0.375$). Thus in a practical situation, one could use very thin vanes near the onset of the corrugations and thicker vanes (which are easier to construct) further from the onset of the corrugations. These curves then establish the length of corrugated horn required to reduce the edge diffracted fields. Since the current density at the top of the teeth is almost zero (see Appendix B) only a few teeth would be required here. For the $3/8\lambda$ depth, the currents at the top of the tooth would be 3 dB below those at the bottom. Thus the illumination of the distant end of the horn would be -15 dB for $x \geq 16$ cm $= 2\lambda$ for $W/TC > 0.7$. Thus the fields of the diffracted ray ("a" of Fig. 1) that phase constructively and destructively with the geometrical optics fields are reduced to a negligible value with a surface that is two wavelengths in extent.

Another property of the corrugated surface which was investigated is the power loss in the corrugations (both the total loss and also the location of regions where the maximum loss occurs). In an effort to make the results more general, the corrugated surface loss is normalized with respect to the loss in an equal size segment of an infinite groundplane of the same material. This eliminates the need to assume a surface resistivity for the material. The results shown in Fig. 10 show the normalized loss in dB versus corrugation number "N" for various corrugation depths. The loss in the corrugated surface is the sum of the loss in each corrugation from the onset of the corrugations (at the origin of the coordinate system) up to and including the loss in the $N^{th}$ corrugation. The loss in the groundplane (used for normalization) is the loss in the region from the origin up to the X-coordinate of the end of the $N^{th}$ corrugation. Notice that most of the loss occurs in the first few corrugations and also that it appears that all of the curves (except the $0.5\lambda$ deep case) would cross the 0 dB line (equal loss in corrugations and groundplane) after a reasonable number of corrugations (the $0.3125\lambda$ and $0.375\lambda$ deep cases cross in fewer than 20 corrugations). The power loss is also dependent upon the corrugation density and shape. Figures 11 and 12 show the power loss in $0.25\lambda$ and $0.375\lambda$ deep corrugations for various corrugation densities. This loss is the loss in the corrugations from the origin to "X" normalized with respect to the loss in the same length segment of an infinite groundplane. Notice that the lower densities are less lossy than the high density surfaces. This result is reasonable in view of the fact that the surface current decay per wavelength is nearly independent of the corrugation density (c.f., Figs. 6 and 7). Thus the higher corrugation density with its greater surface area should be more lossy. The influence of the corrugation shape on the power loss may be seen in Figure 13.

Shown here is the loss in 20 corrugations (from x = 0 to x = 20 cm) normalized with respect to a 20 cm segment of an infinite groundplane versus the corrugation depth (D/λ) for various W/TC ratios. The W/TC = 0.5 case corresponds to a thick metal vane between corrugations while the W/TC = 0.9 case corresponds to a very thin vane. Notice that the thin vanes have lower loss than the thick vanes and that there exists a range of depths over which the loss is minimized.

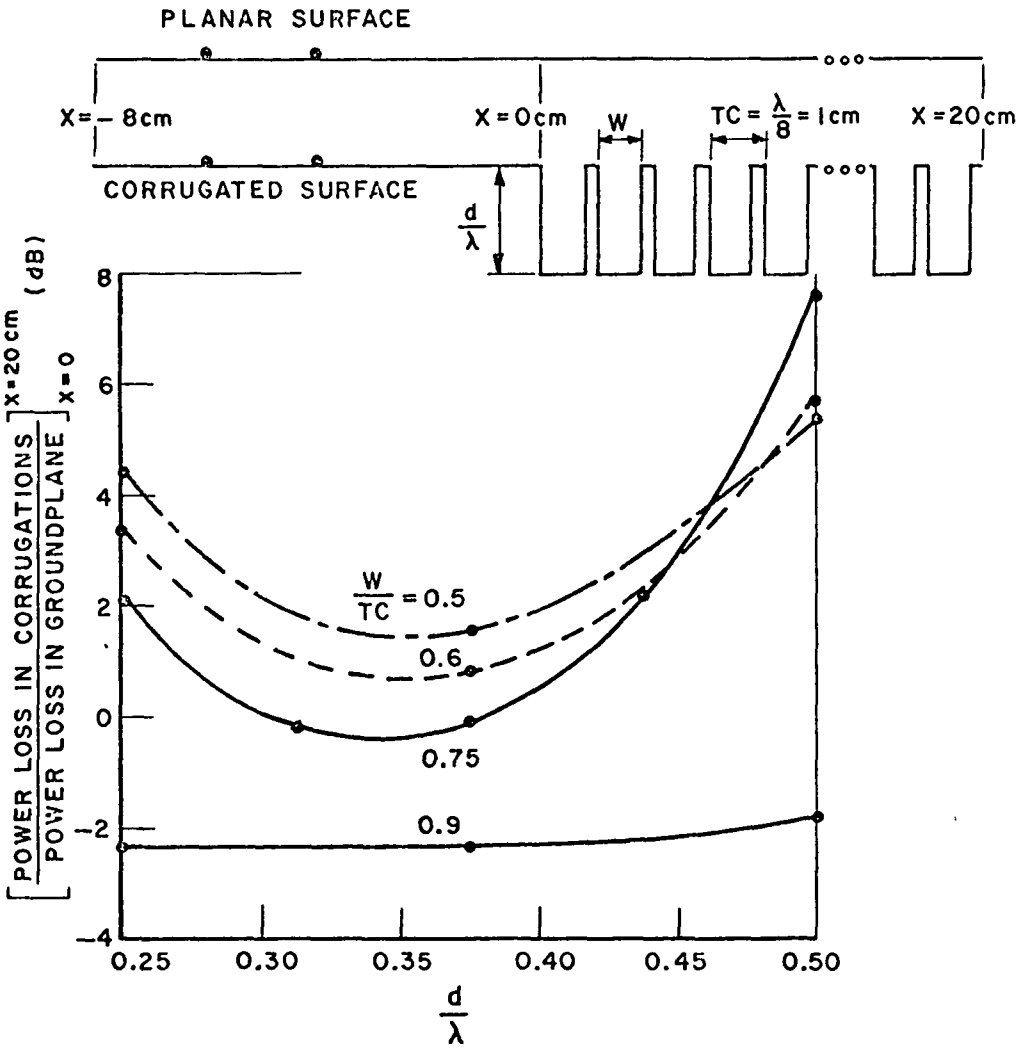


Fig. 13. Power loss in 20 corrugations versus corrugation depth for various corrugation profiles.

The general conclusion which might be drawn at this point is that corrugation density and tooth shape can be selected to optimize the performance of a corrugated horn by a) choosing as few corrugations as four/wavelength, b) by making the vanes as thin as is practical. However, there is one final parameter that must be considered. The impedance of the horn would be related to the magnitude of the wave reflected back toward the source. The computer programs developed here are not well designed to evaluate this reflection coefficient. However, they can be used to obtain an indication of this parameter. The current on the groundplane region of Fig. 2a can be expressed in the following form:

$$\bar{J} = \bar{J}_s + \bar{J}_1 + \bar{J}_2 \tag{7}$$

where $\bar{J}_s$ is the current density of the source when placed on an infinite conducting plane,
$\bar{J}_1$ is the current density associated with the wave reflected by the onset of the corrugations, and
$\bar{J}_2$ is the current density associated with the waves reflected by the end of the groundplane.

Since the two line sources are phased to give zero far field in the $\theta = \pi$ direction, and since the diffraction coefficient associated with the back scattered field at this edge is small, $\bar{J}_2$ may be neglected. When the observation position is sufficiently removed from the edge, the current density $\bar{J}_1$ will decay as $1/\sqrt{r}$ since it is caused by the radiation of a line source. Thus the equation for the surface current has the form:

$$\bar{J} = \bar{J}^s + 2\bar{n} \times \bar{H}_0/\sqrt{r} \tag{8}$$

where $r$ is the distance on the groundplane from the onset of corrugations. Since $\bar{J}^s$ is known exactly, $\bar{J}_1$ can be found with reasonable accuracy. Its representation as $2H_0$ is, of course, only approximate. A plot of $|H_0|$ versus the corrugation depth is shown in Fig. 14 for the W/TC = 0.75, 8 corrugations per wavelength case. As previously discussed, the $\lambda/4$ depth has a large reflected wave associated with it. The reflection from the junction also depends on the tooth shape and density. Figures 15 and 16 show $|H_0|$ versus corrugation density and profile ratio respectively. Notice that at both $\lambda/4$ and $3\lambda/8$ depths, the higher corrugation density and thick teeth (W/TC = 0.5) have lower reflections associated with them. The W/TC = 0.9 points in Fig. 16 are shown with a dashed line as some difficulties were noticed for cases where matching segments were very close together. This is probably the case for the W/TC = 0.9 data.

A general observation is that the impedance as a function of corrugation density would require as many corrugations as possible in order that the VSWR be maintained low over the largest possible bandwidth.

Now we arrive at the optimum design of the corrugated surface in terms of expense, and operation. There should be from 8 to 12 corrugations over the first wavelength. These teeth should be as thin as is possible for low loss. Then the tooth density should be tapered to 4 per wavelength and

the tooth width should be increased to W/TC = 0.5. In addition, the first few teeth should be plated to further reduce losses. Also, for low loss, the waveguide and throat region of the horn should be plated regardless of whether the horn is corrugated or not.

However, if loss is not an important consideration, then the reflection coefficient and consequently the horn VSWR should be minimized by increasing the corrugation density to at least 8 corrugations per wavelength. The reflection coefficient can also be reduced by initiating the corrugation at a point further removed from the horn waveguide junction. However, one must be certain to initiate the corrugations before a second mode could be excited in the horn[4].

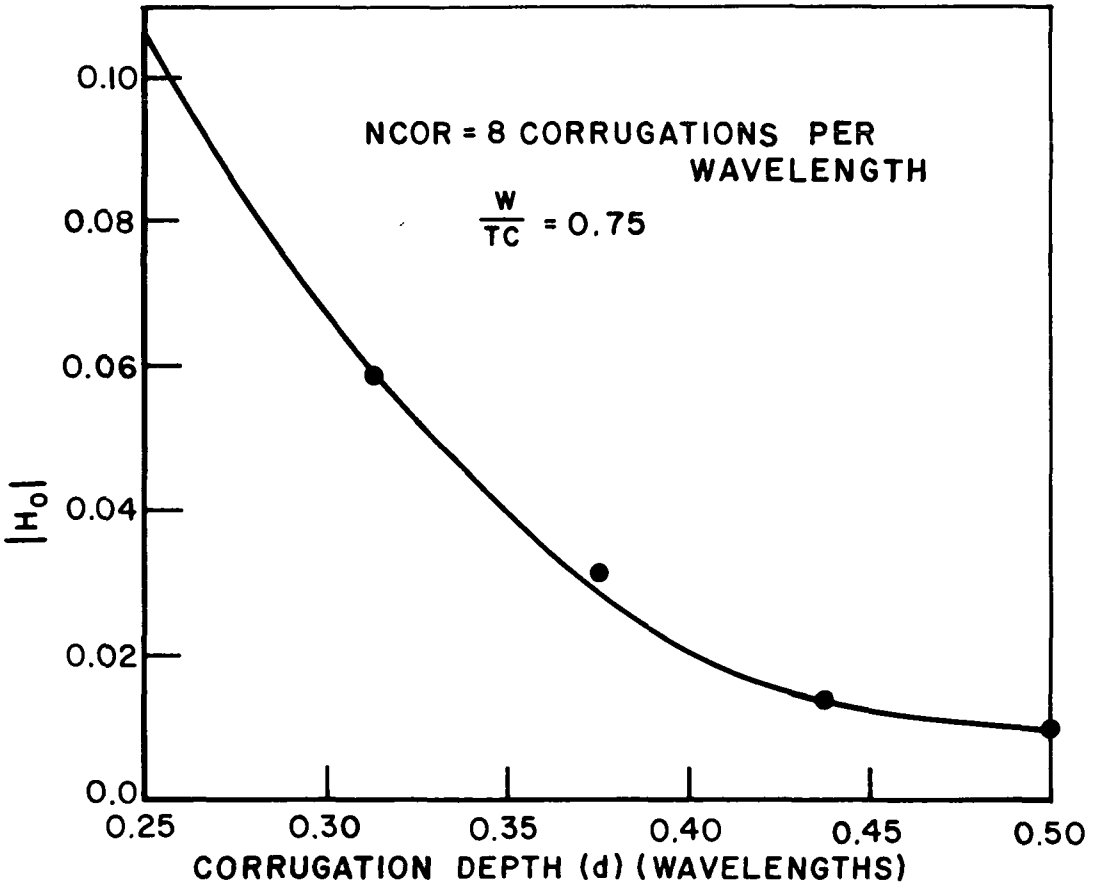


Fig. 14. $|H_0|$ versus corrugation depth.

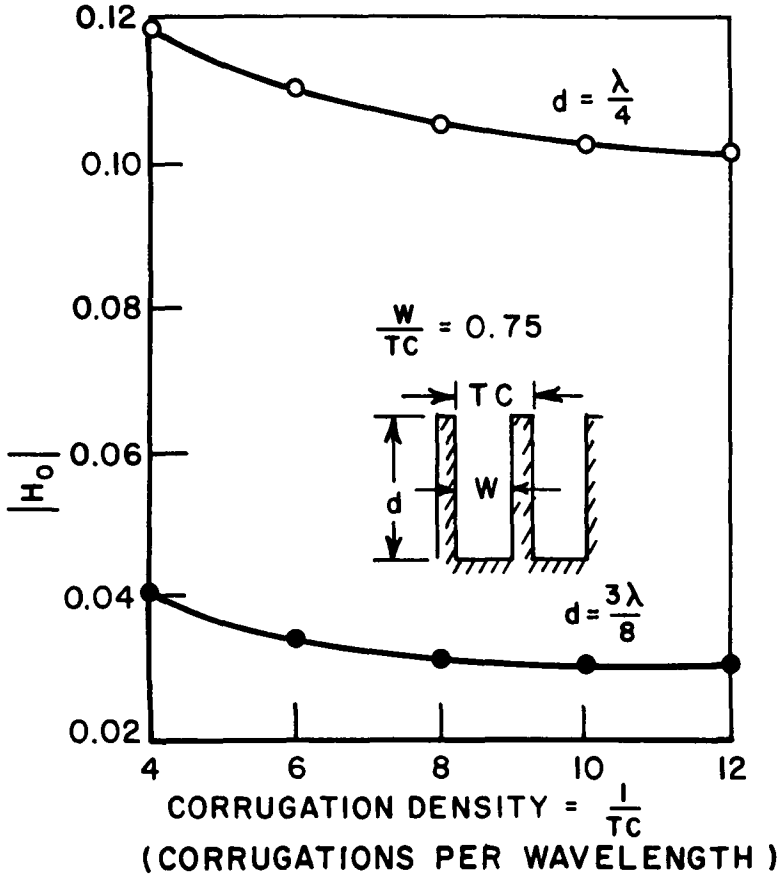


Fig. 15. $|H_0|$ versus corrugation density.

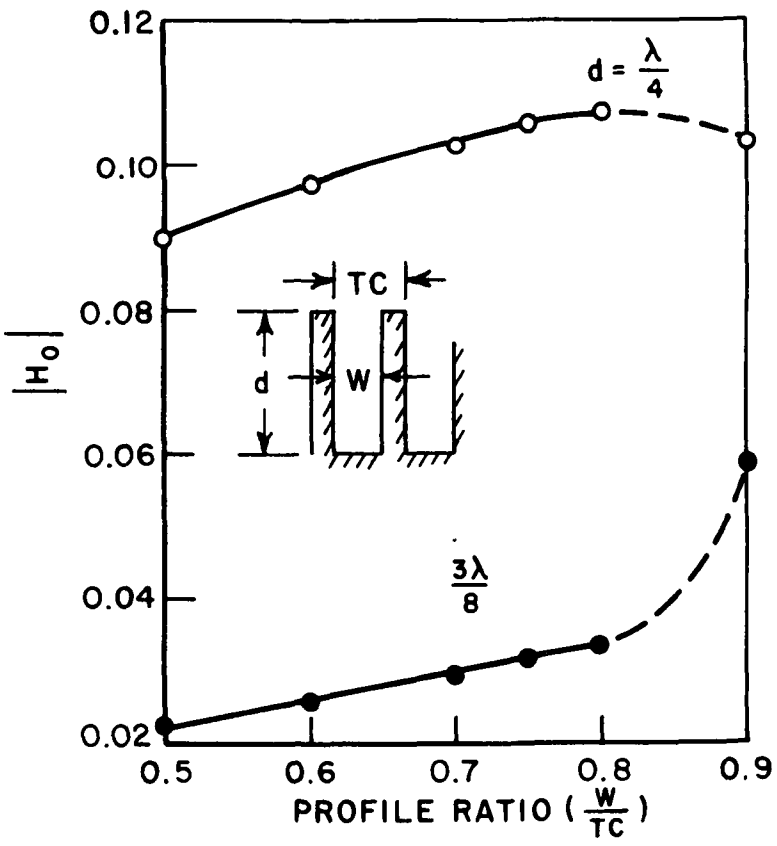


Fig. 16 $|H_0|$ versus corrugation shape.

## IV. RESULTS FOR VEE CORRUGATIONS

The study of the vee corrugations shown in Fig. 2b was undertaken because there are situations where the square shape of the previous section is impractical or unsuitable. The thin vane of the square corrugation is impractical at frequencies much above 12 GHz because of the difficulty encountered in machining or extruding the corrugations. The difficulty should be eliminated with the V-shape corrugation. Also, the square shape is not as suitable as the V-shape for an application where the surface needs to fold or collapse in order to take up less space. Using an asymmetric V-shape, an unfurlable corrugated horn antenna which would fold like a camera bellows is practical. The corrugated surfaces considered in this section have symmetric V-shape corrugations defined by the corrugation depth, $d/\lambda$, and the corrugation density, NCOR (in corrugations per wavelength). The range of parameters presented for the V-shape is not as complete as for the square shape because of some problems encountered in calculating the surface currents for the deep corrugations and for high corrugation densities (NCOR 8). These cases will not be reported here. It is believed that for these cases, the coupling coefficient between adjacent segments at the top or bottom of each corrugation is erroneous because of the very small distance between the matching points. A sufficient number of cases are available to indicate that the V-shape does operate as a cut-off corrugated surface for corrugation depths from $0.3125\lambda$ to about $0.625\lambda$. Cut-off operation of a corrugated surface requires a capacitive surface impedance. That the surface impedance of the vee corrugation is capacitive over most of this range of depths has been verified using Harrington's results for the fields in a wedge shape waveguide with radial propagation[12]. The impedance looking into the wedge waveguide is:

$$(9) \qquad Z = jZ_0 \, J_1(k\rho)/J_0(k\rho)$$

where $\rho$ is the radial distance from the bottom of the corrugation. For the deep, narrow corrugations being considered, this yields an operating range of approximately $0.382 \leq d/\lambda \leq 0.605$. This operating band is narrower than the computer calculations indicated but then the wedge radial waveguide is only an approximate model for the V-shape corrugations. The results of the computer calculations are discussed next.

Figure 17 shows: a) the groundplane matching points, b) the surface current magnitude, and c) the surface current phase in the source region. Figure 17b shows the physical optics current (on an infinite groundplane) and the approximate current representation for the computer selected match points. Both the amlitude and phase are accurately modeled for this point selection.

The properties of the vee corrugations which were studied include the radiation patterns of the surface model, the surface currents in the corrugations, and the power loss in the corrugations. Figure 18 shows the radiation pattern (total magnetic field) of the surface model shown in the insert and in Fig. 2b for several vee corrugation depths. As with the square corrugations, the radiation pattern is nearly independent of the corrugation density (i.e., the pattern at a given depth is nearly identical for the 4, 6,

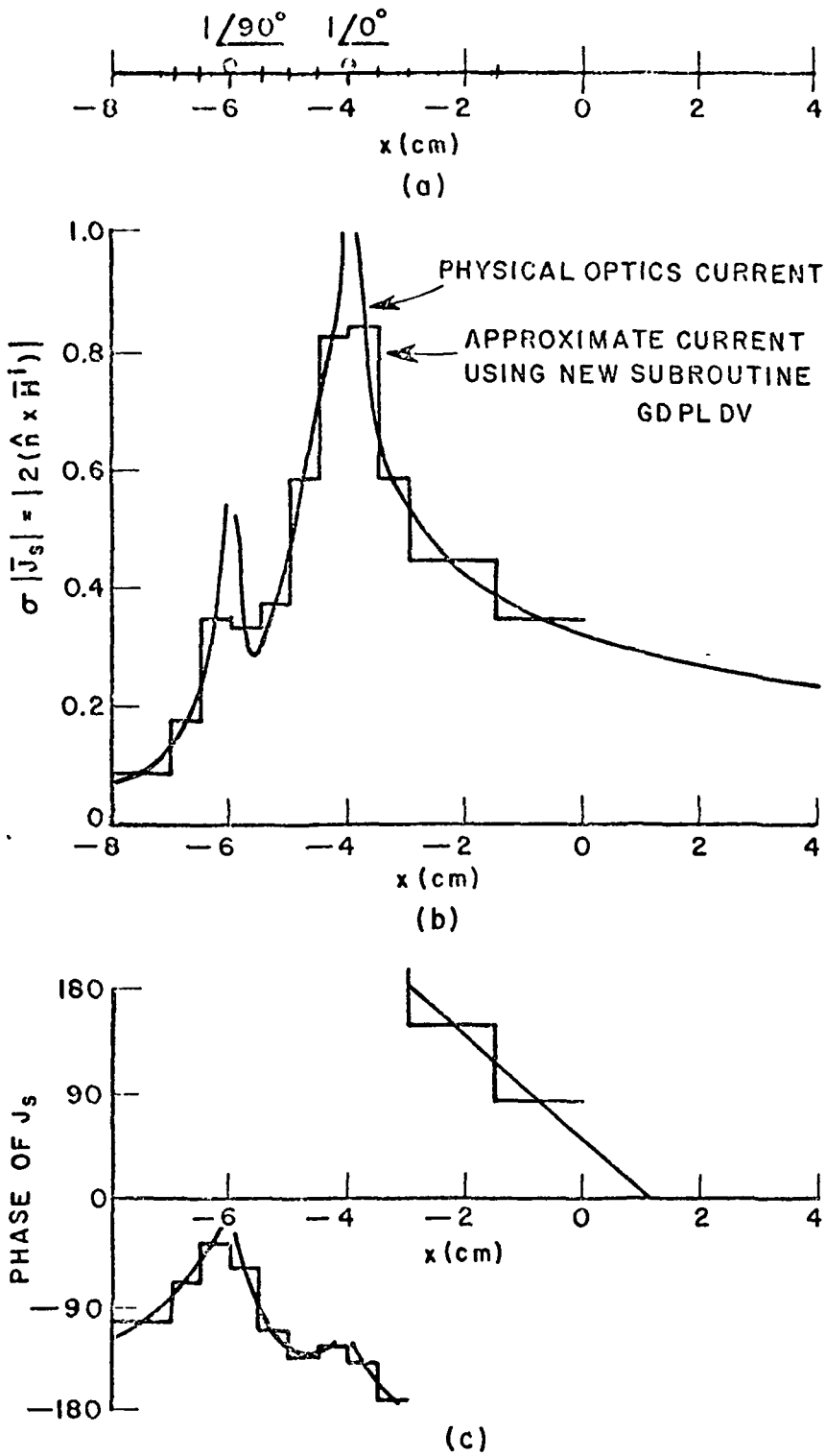


Fig. 17. Surface currents near the line sources used to model the groundplane-corrugated surface junction a) matching points on groundplane, b) surface current magnitude, and c) surface current phase.

or 8 corrugations per wavelength cases) and the direction of maximum intensity decreases with increasing corrugation depth.

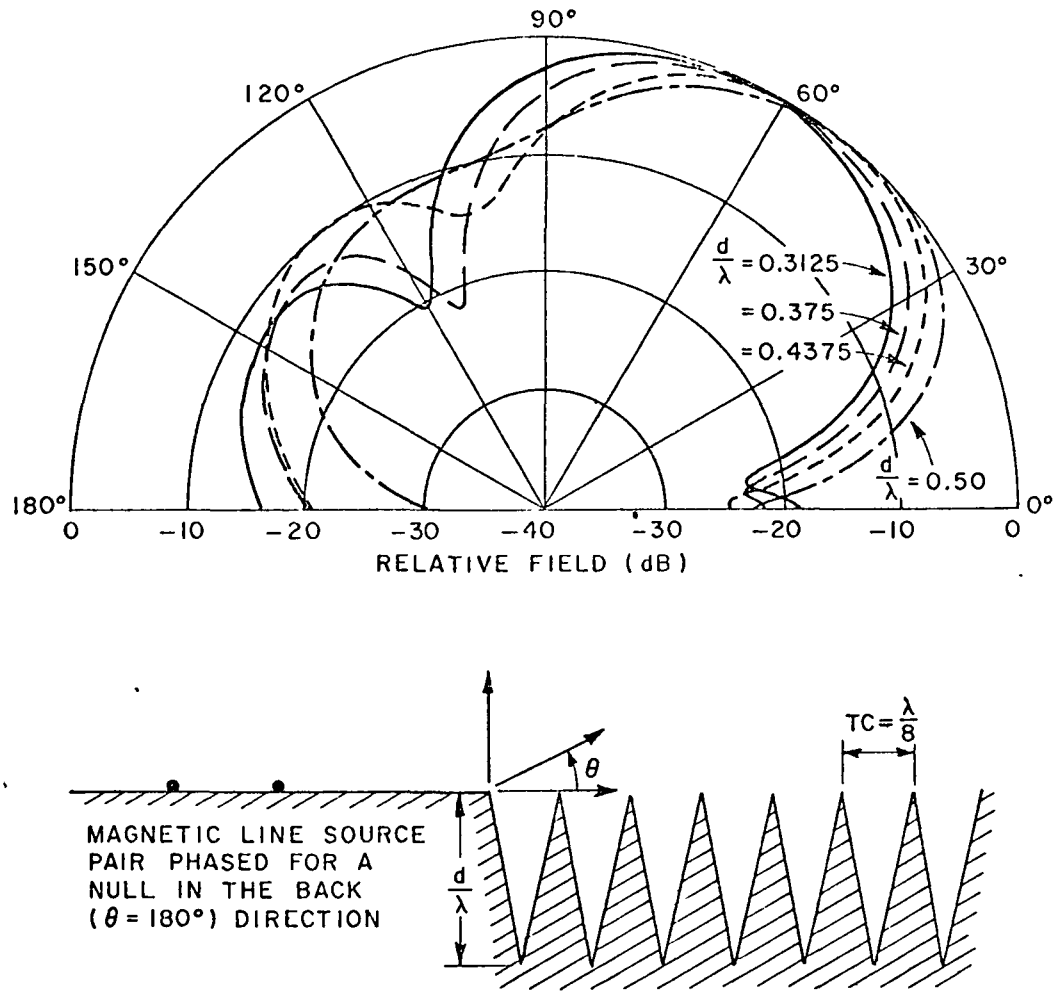


Fig. 18. Radiation pattern of a groundplane-vee corrugation junction illuminated by a cylindrical wave.

Other similarities between the V-shape and the square corrugations are found in the surface current decay and power loss. Figures 19, 20, and 21 show the surface current (in dB) which exists near the bottom of the vee corrugations normalized with respect to the surface current which exists at the same "X" coordinate on an infinite groundplane with the same sources acting. Figure 19 shows this current versus the distance (in wavelengths and in cm) from the onset of the corrugations for two corrugation depths near the low end of the operating band. At the lowest frequency in the cut-off band

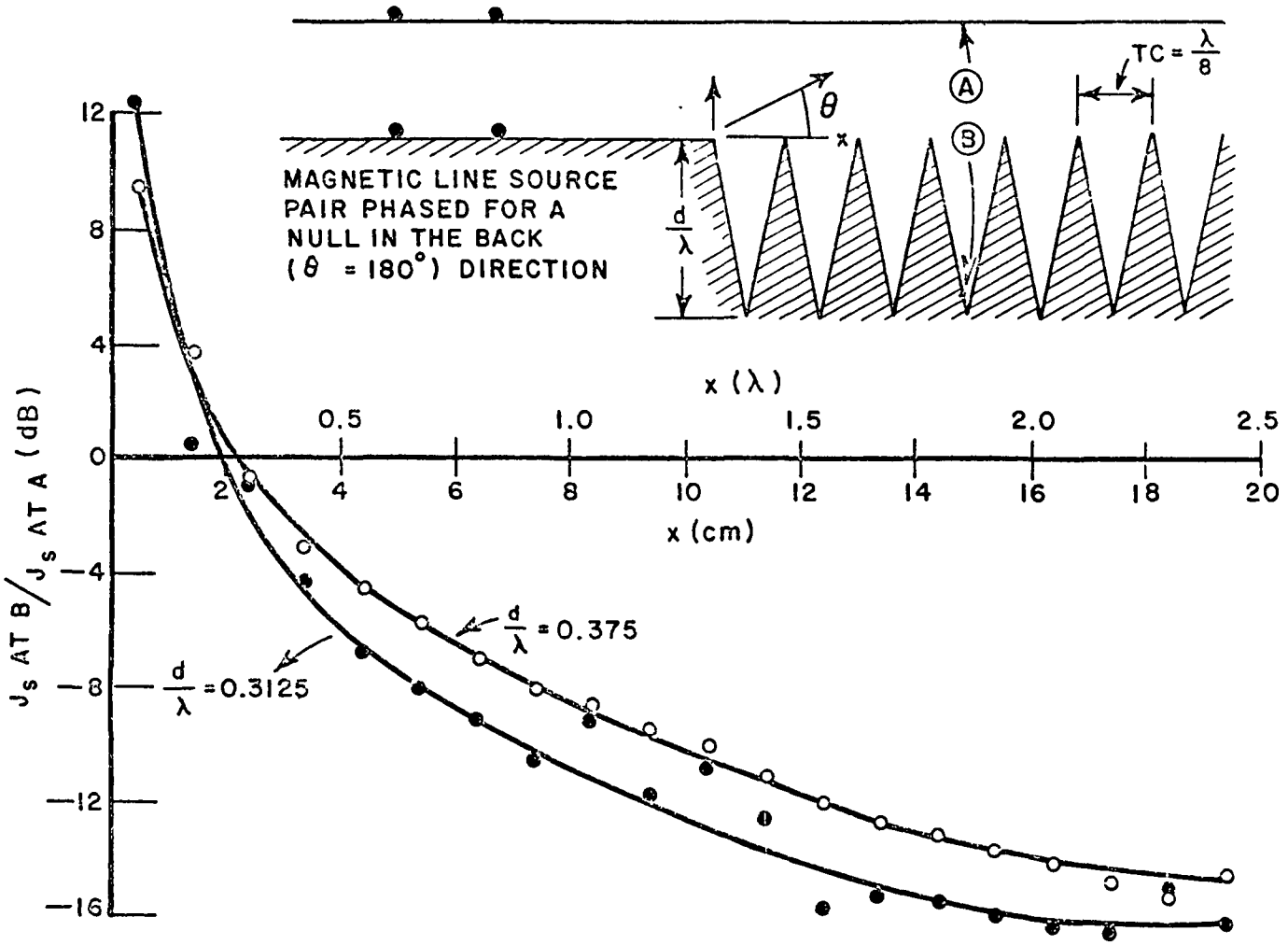


Fig. 19. Relative surface current on vee corrugations versus distance from the onset of the corrugations.

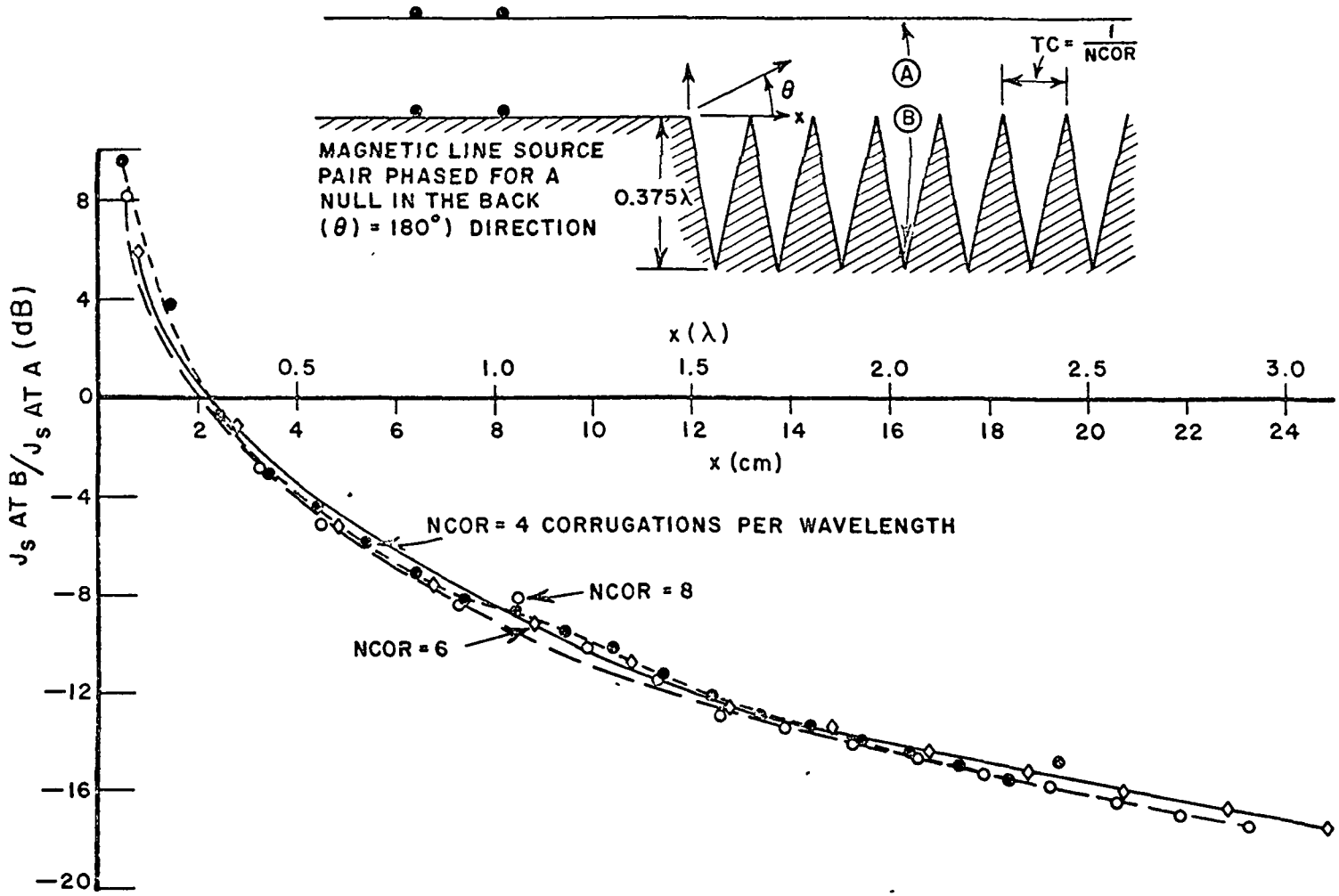


Fig. 20. Relative surface current on 0.375λ deep vee corrugations versus the distance from the onset of the corrugations for several corrugation densities.

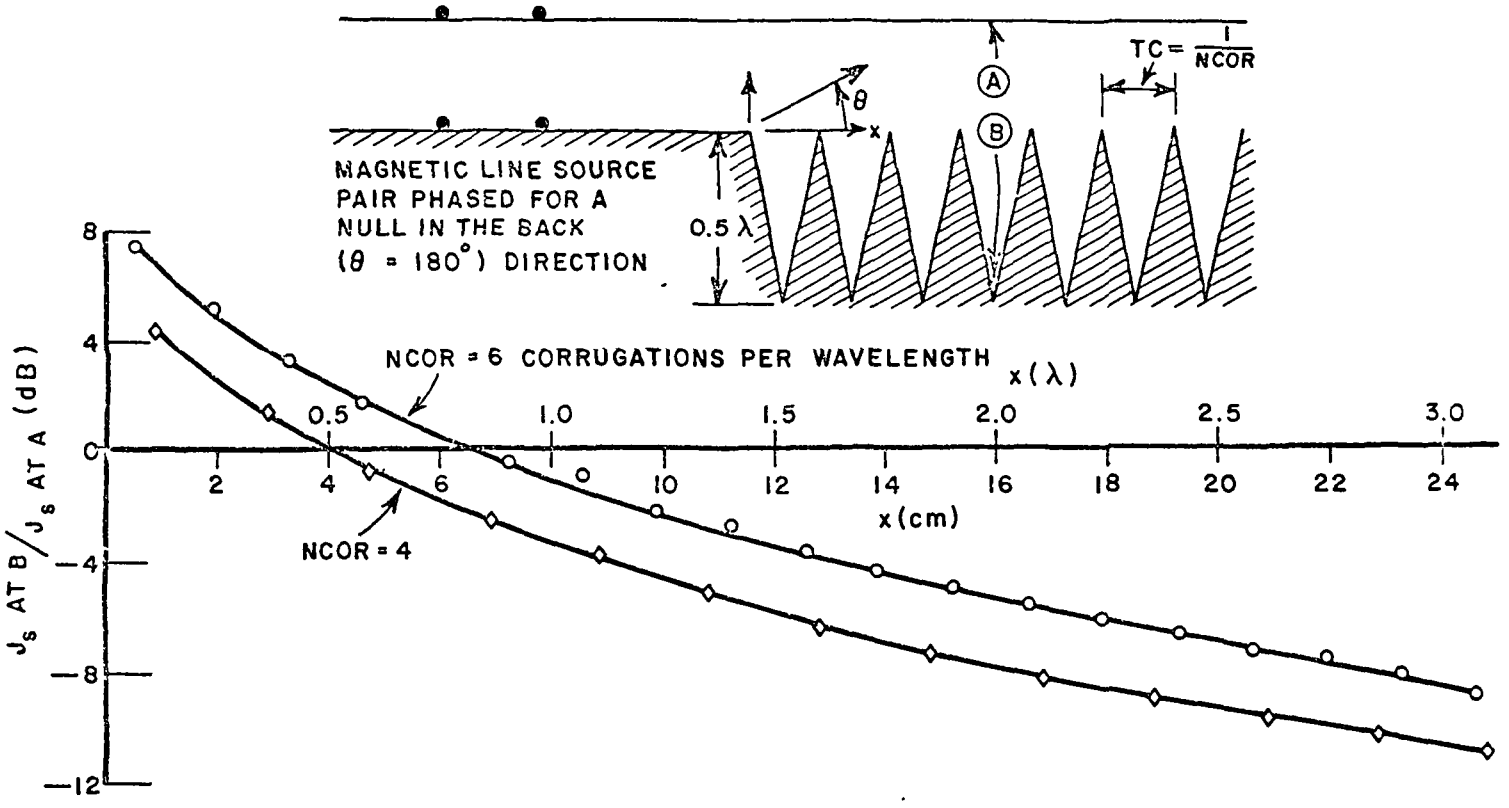


Fig. 21. Relative surface current on 0.5 deep vee corrugations versus the distance from the onset of the corrugations for several corrugation densities.

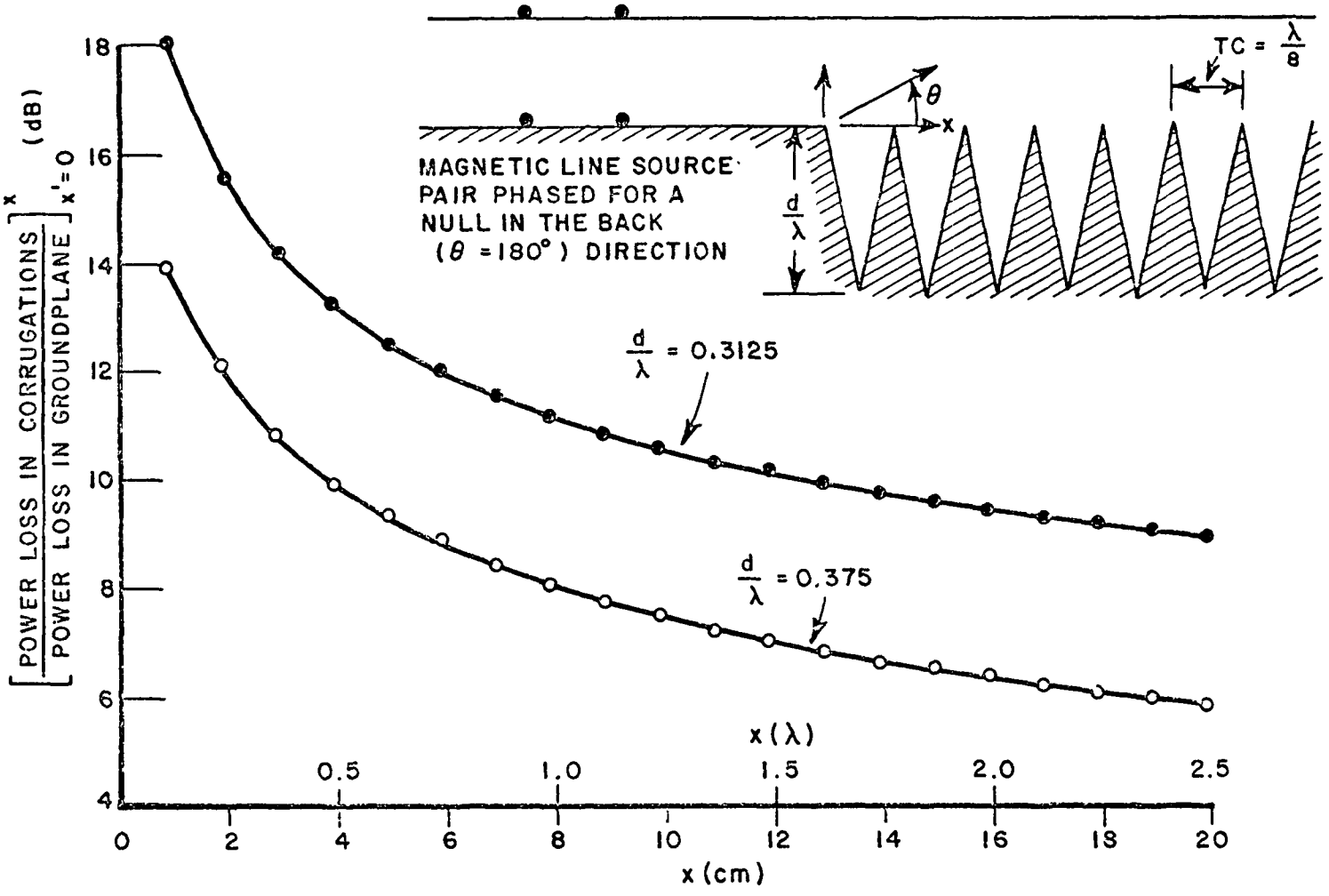


Fig. 22. Relative power loss in vee corrugations from origin to "X" (normalized with respect to the loss in 0→X segment of infinite groundplane) for two corrugation depths.

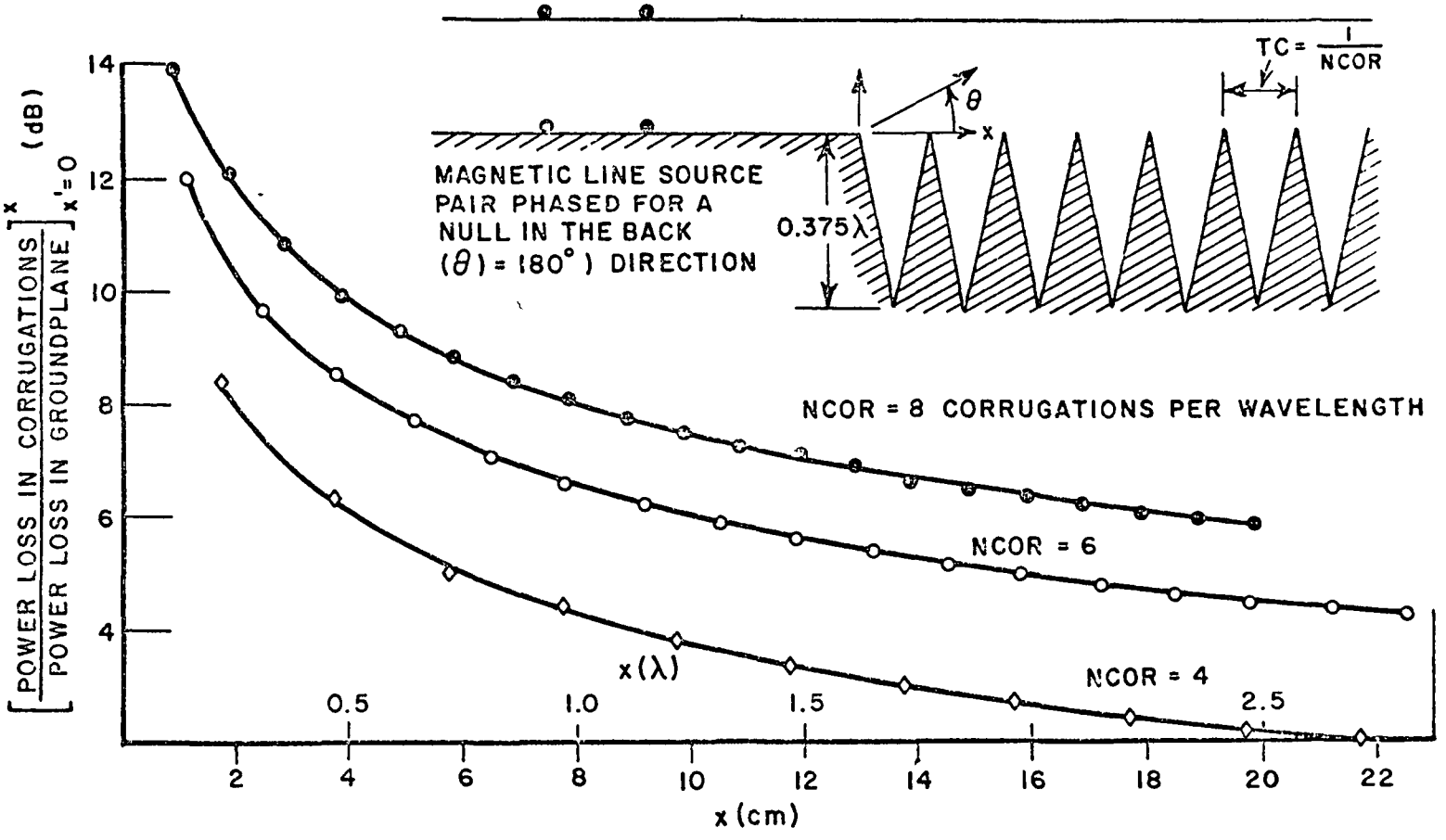


Fig. 23. Relative power loss in 0.375 deep vee corrugations from origin to "X" (normalized with respect to the loss in 0→X segment of infinite groundplane) for three densities.

($d/\lambda = 0.3125$), the surface current decay along the vee corrugated surface is nearly identical to that of the square corrugations at the lowest frequency in its band (c.f., $d/\lambda = 0.25$ in Fig. 5). As was the case for the square corrugations, the surface current decay is most rapid at the low end of the frequency band. Figures 20 and 21 show similar current curves for various corrugation densities at depths of $0.375\lambda$ and $0.5\lambda$ respectively. Notice that near the lower end of the operating band the surface current decay is independent of the number of corrugations per wavelength while near the upper end of the band there is some dependence on the corrugation density.

Figures 22 and 23 show the relative power loss in the vee corrugations. The loss which is plotted is the loss in the corrugations from the origin to the "X" coordinate normalized with respect to the loss in the same length segment of an infinite groundplane. Figure 22 shows the loss at the two lowest frequencies for the 8 corrugations per wavelength case. The loss here is higher than the square corrugations because of the higher surface current near the point of the vee and also because of the greater arc length in the V-shape surface. Figure 23 shows the loss at $d/\lambda = 0.375$ for 4, 6, and 8 vee corrugations per wavelength. As with the square corrugations, the lower corrugations density has the lower loss. Because of the higher current (and consequently higher loss), if one is to use the V-shape corrugations in a situation where low loss is important something such as polishing or silver plating the first few corrugations should be considered. For an unfurlable horn, the first part of a horn might be rigid and use square corrugations to obtain lower loss while the remainder of the horn could be an unfurlable geometry using triangular teeth. Also, because the current in the corrugations become very small after 4 or 5 corrugations the loss in the corrugations will eventually become smaller than the loss in the groundplane.

## V. CONCLUSIONS

A parametric study of square and vee corrugations has shown that both shapes operate as cut-off corrugated surfaces over subtantial bandwidths with relatively low loss. The study has also shown that the rate of decay of surface current is nearly independent of the corrugation density (the number of corrugations per wavelength and that the lower corrugation densities (4 or 6 corrugations per wavelength) are desirable because of the lower loss. A significant part of the loss is confined to the first few corrugations and should allow one to treat this region with special care such as silver plating or special polishing of the surface when using corrugated surfaces in situations where low loss is important. In any event, the loss in the walls for most practical corrugated horns would be as low as (if not lower than) the loss in the same shape and size conducting wall of the same material with the same surface finish. The results also indicate that the VSWR of the horn will depend on the corrugation shape. For the groundplane-corrugated surface junction considered, the VSWR decreased with increasing corrugation density and increased with thinner teeth between the corrugations. Since the loss increases with increased corrugation density, some compromise is required. Six to eight corrugations per wavelength near the onset of the corrugations and then decreasing the density to two to four per wavelength should be adequate. Again, since the loss was lower and the VSWR higher for the very thin teeth, some compromise is also indicated A corrugation width

to period ratio of W/TC = 0.75 should be a good compromise value if one wants to avoid the complexity of changing the corrugation shape along the corrugated wall.

While this work has yielded considerable insight about corrugated surface design, there remain several sets of important design data that can be obtained with a similar approach. For example, the sources on the groundplane should be moved off the groundplane and the corrugated surface performance analyzed for various source locations. This would simulate the fields incident on the corrugations due to the diffraction from the horn-waveguide junction and the onset of the corrugations on the opposite wall of the horn. Also, the groundplane should include a corner similar to the horn-waveguide junction. Ideally, the entire horn should be considered. This has been programmed using the integral equation approach but is of limited value because of the extremely small horn which can be handled due to computer storage limitations. Using image techniques and other procedures currently being developed at the ElectroScience Laboratory, it should be possible to consider 10 or more corruagtions in this model for VSWR computations. This number of corrugations should provide adequate reduction of the surface current at the top of the last corrugation to obtain valid calculations for realistic horn throat geometries. For the corrugated horn pattern, a diffraction coefficient could be associated with the scattering from the onset of the corrugations using the integral equation approach. Then, using the techniques of the Geometrical Theory of Diffraction, one could proceed to obtain full horn patterns including the back lobe radiation.

## APPENDIX A

## COMPUTER PROGRAM USED FOR CORRUGATED SURFACE ANALYSIS

The main computer program and the subroutines required to solve the set of equations obtained from the integral equation of section II by point matching will now be briefly discussed. The program and subroutines are written in the Fortran IV language. The main program listing is at the end of this section. The input parameters to the main program are contained on two cards: the first specifies the corrugation shape, and the second the groundplane and corrugated surface dimensions. The data on the first card is grouped into five groups of (F8.3,I2) fields. Each group locates a corner (in F8.3 field) and specifies the number of segments (in I2 field) to be placed on the line from the previous point to the current point. Figure A1 shows a typical period or cell from a corrugated surface of period TC = 1/NCOR where NCOR is the corrugation density (in corrugations per wavelength).

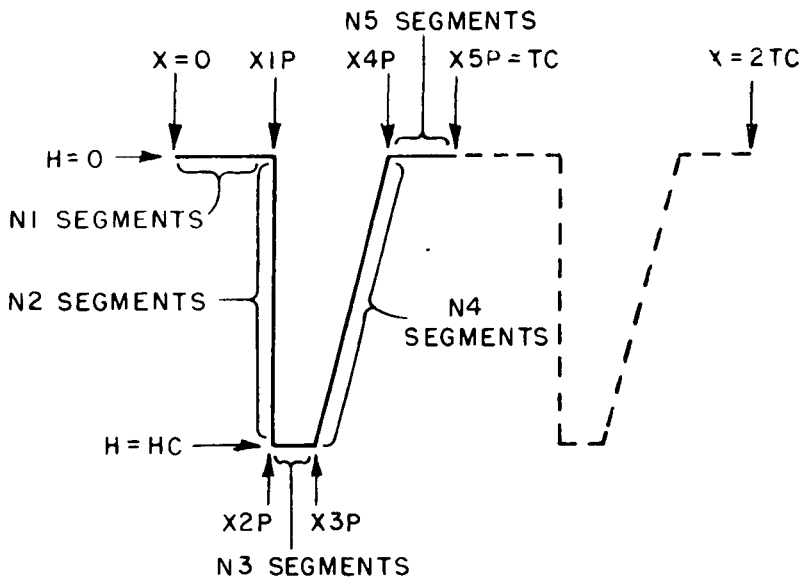


Fig. A1

The X1P to X5P are expressed as ratios normalized to the corrugation period TC with X5P = TC. The heights of the corners are assumed to be either H = 0 or H = -HC as shown. Additional information on these parameters is contained in the discussion of the VSURDV subroutine. The remaining input parameters are shown in Fig. A2 and listed below:

EPL locates the end point on the left or groundplane side in cm.,
NGP specifies the number of matching segments to be placed on the groundplane side of the origin,

EPR locates the end point on the right or corrugated surface side of the origin (in cm.),
WE is the electrical wavelength (in cm.),
HCWE is the height of the corrugations in wavelengths,
NCOR is the number of corrugations per wavelength, and
KSET is an identifier for the set of data and is not used in any calculations.

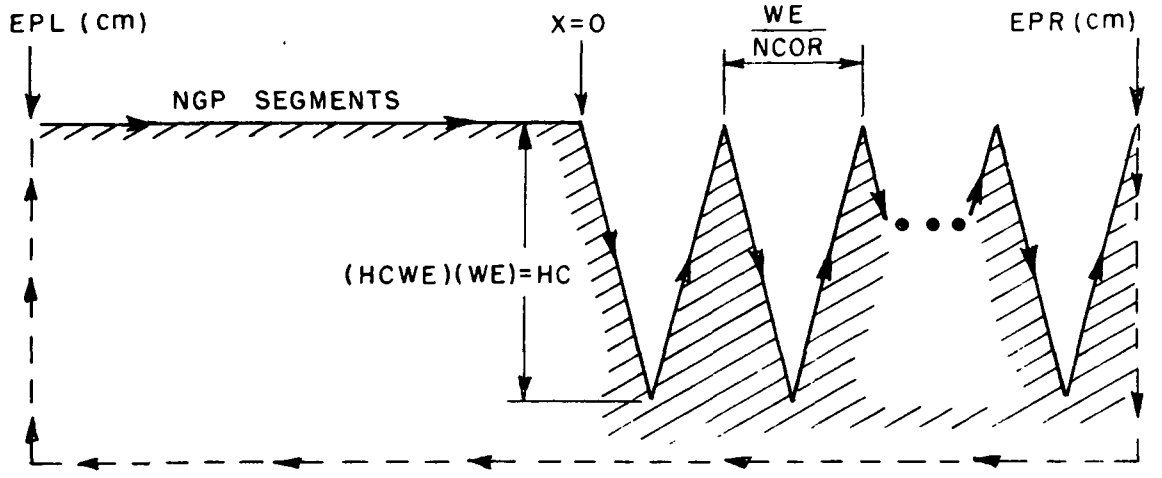


Fig. A2

Also shown in Fig. A2 as a broken line is the path used for closing the body to check the validity of the open surface model. The body is closed by setting the last calling parameter in the CALL VSURDV (line 36 of the main program listing) to 1 rather than 0 (open body). The match points on the groundplane and corrugated surface are determined by calling the GDPLDV and VSURDV subroutines in this order (lines 35 and 36 in the listing). These subroutines are discussed later. The output includes a list of the "X" and "H" coordinates of the match points, the direction of the surface normals, and the length of each segment as determined by these subroutines (line 39). Also listed as output is the incident field on each segment (line 74) and after the matrix inversion, the surface current on each segment (line 82). Also plotted are the magnitude (line 88) and phase (line 93) of the surface current versus segment number and the radiation zone magnetic field pattern versus the observation angle (line 122). In addition to these plots the magnitude and phase of the scattered field and the total field are listed versus $\theta$(line 12 ). Finally, the relative power loss is summed and listed versus the segment number (line 136). The Fortran listing follows.

```
C      TE CASE  GAUSSIAN INTEGRATION USED TO FILL IN MATRIX
C      TE CASE  GAUSSIAN INTEGRATION USED TO FILL IN MATRIX
       COMPLEX HINC,HTC,HNORM
       COMPLEX ESS,S,CO,SNN,SST
       COMPLEX SS,T,CTEST,FIN,HAN2,DJC,STS
       COMMON /DOG/ DJC
       DIMENSION         ARES(360),Y(10),HTOT(360)
       COMMON /MAWIGD/ DZ1,DZ2
       COMMON/MAINDV/ X(230),H(230),TN(230),SEGL(230),DEL,HC,G,EPL,EPR,WE
       COMPLEX FINC(230),C(230,230),F(230)
       NDIM=230
C      WE  IS THE ELECTRICAL WAVELENGTH
C SOURCE LOCATIONS
       DZ1=-4.0
       DZ2=-6.0
       READ(5,1) X1P,N1,X2P,N2,X3P,N3,X4P,N4,X5P,N5
    1  FORMAT(5(F8.3,I2))
       READ(5,2) EPL,NGP,EPR,WE,HCWE,NCOR,KSET
    2  FORMAT(F10.4,I5,3F10.4,I5,25X,I5)
       WRITE(6,9997) EPL,EPR,WE,HCWE,NCOR,NGP
 9997 FORMAT(' GROUNDPLANE FROM ',F10.4,' CM TO ORIGIN, VEE CORRUGATION
     2S FROM ORIGIN TO ',F10.4,' CM'/' WAVELENGTH=',F10.4,' CM'/' CORRUG
     3ATION HEIGHT=',F10.4,'WAVELENGTHS'              /I5,'CORRUGATIONS
     4PER WAVELENGTH'/I5,' POINTS ON GROUNDPLANE')
       PI=3.14159
       P12=PI/2.
       RDEG=180./PI
       TC=WE/NCOR
       X1=X1P*TC
       X2=X2P*TC
       X3=X3P*TC
       X4=X4P*TC
       X5=X5P*TC
       HC=HCWE*WE
       CALL GRPLDV(NGP,MP)
       CALL VSURDV(X1,X2,X3,X4,TC,N1,N2,N3,N4,N5,MP,0)
       N=MP-1
       WRITE(6,20)
       WRITE(6,21)(M,X(M),H(M),TN(M),SEGL(M),M=1,N)
    20 FORMAT(T4,'M',T15,'X',T30,'H',T45,'TN',T60,'SEGL')
    21 FORMAT(I5,4F15.4)
       IF(N.LE.NDIM) GO TO 19
       WRITE(6,18) N
    18 FORMAT(' N=',I5,' EXCEEDS DIMENSION OF C')
       CALL EXIT
    19 CONTINUE
       G=6.2831853        /WE
       STS=   -CMPLX(0.707107,0.707107)/(2.0*SQRT(WE))
       DJC=CMPLX(0.0,1.0)*G/4.0
       NM0=N-1
       NM3=N-3
       DPIF=0.7853982
C      MATRIX FILL IN
       DO 3661 IR=1,N
       DO 3661 IC=1,N
 3661  C(IR,IC)=CO(IR,IC)
C     THIS COMPLETES THE FILLIN OF THE MATRIX
       WRITE (6,1222) N,WE
 1222  FORMAT(3H N=,I3,4H WE=,E15.8)
C      THIS FINDS THE INCIDENT FIELD ION THE NJTH SEGMENT
       DO 455 NJ=1,N
       XG=0.50*(X(NJ)+X(NJ+1))
C      THE SIGN ON THE INCIDENT FIELD HAS BEEN ADJUSTED TO AGREE WITH
C      THE INTEGRAL EQUATION
       HG=0.500*(H(NJ)+H(NJ+1))
```

```
      RHO=SQRT(XG*XG+HG*HG)
      PHI=ATAN2(HG,XG)*RDEG
      CALL WILLUM(RHO,PHI,HINC,WE)
      FINC(NJ)=-HINC
      F(NJ)=FINC(NJ)
  455 CONTINUE
      WRITE(6,2947)
 2947 FORMAT(/5H     M,10X,16H INCIDENT FIELDS )
      WRITE(6,2948) (NJ,FINC(NJ),NJ=1,N)
 2948 FORMAT(I5,E15.8,4H +J ,E15.8)
      CALL CROUTN(C,F,N,NDIM)
      WRITE(7,9300)(KSET,M,X(M),H(M),TN(M),SEGL(M),F(M),M=1,N)
 9300 FORMAT(2I5,4F10.4,2E15.8)
      DO 554 IKUR=1,N
      AAF=CABS(F(IKUR))
      ANF=57.296*ATAN2(AIMAG(F(IKUR)),REAL(F(IKUR)))
  554 WRITE(6,553)IKUR,AAF,ANF
  553 FORMAT (' ','F(',I4,')=', E15.8,'   AT ANGLE=',E15.8)
      DO 9553 IRRO=1,N
      IND=IRRO-1
      Y(1)=CABS(F(IRRO))
      XRRO=FLOAT(IRRO)
 9553 CALL PLOT(XRRO,Y,1,IND,5.00,0.0)
      DO 9554 IRRO=1,N
      IND=IRRO-1
      Y(1)=57.2958*ATAN2(AIMAG(F(IRRO)),REAL(F(IRRO)))
      XRRO=FLOAT(IRRO)
 9554 CALL PLOT(XRRO,Y,1,IND,180.0,-180.0)
      RHO=200.
      HNORM=2.*CEXP(CMPLX(0.,-2.*PI*RHO/WE))/SQRT(RHO)
      WRITE(6,311)
  311 FORMAT(1H1,7X,16HRELATIVE H FIELD,33X,13HTOTAL H FIELD /2X,9HMAGNI
     2TUDE,6X ,5HANGLE, 7X,2HDB,8X,5HTHETA,9X,2HDB,6X,9HMAGNITUDE,7X,
     3 5HANGLE)
      DO 317 JNX=1,180
      THS=0.01745329*FLOAT(JNX)
      T=CMPLX(0.0,0.0)
      DO 310 I=1,N
      XN=0.500*(X(I)+X(I+1))
      HM=0.500*(H(I)+H(I+1))
      THN=TN(I)
  310 T=T+ ((F(I)*CEXP(CMPLX(0.0,G*((XN*COS(THS))+(   HM*SIN(THS))))))
     2 *COS(THN-THS))*SEGL(I)
C     ********** THIS CORRECTS THE OUTPUT TO TRUE MAG. FIELD
      T=T*STS
      CM=CABS(T)
      DB=20.0*ALOG10(CM)
      CANG=57.296*ATAN2(AIMAG(T),REAL(T))
      THSD=THS*57.296
      ABFS(JNX)=CM
      CALL WILLUM(200.,THSD,HINC,WE)
      HTC=T+HINC/HNORM
      HTM=CABS(HTC)
      HTA=RDEG*ATAN2(AIMAG(HTC),REAL(HTC))
      HTD=20.*ALOG10(HTM)
      HTOT(JNX)=HTM
  317 WRITE(6,312) CM,CANG,DB,THSD,HTD,HTM,HTA
  312 FORMAT(E15.8,2F10.4,2X,F10.4,2X,F10.4,E15.8,F10.4)
      DO 9500 JC=1,180
      Y(1)=ABFS(JC)
      Y(2)=HTOT(JC)
      U=FLOAT(JC)
      IND=JC-1
 9500 CALL PLOT(U,Y,2,IND,1.00,0.0)
      PLOSS=0.0
```

```
      WRITE(6,9994)
9994  FORMAT(' POWER LOSS PER UNIT RESISTIVITY'/'     M',5X,'PLOSS')
      DO 9999 LOSS=1,N
      TEMP=CABS(F(LOSS))
      PLOSS=PLOSS+TEMP*TEMP*SEGL(LOSS)
      WRITE(6,9996) LOSS, PLOSS
9996  FORMAT(I5,F15.6)
9999  CONTINUE
      CALL EXIT
      END
```

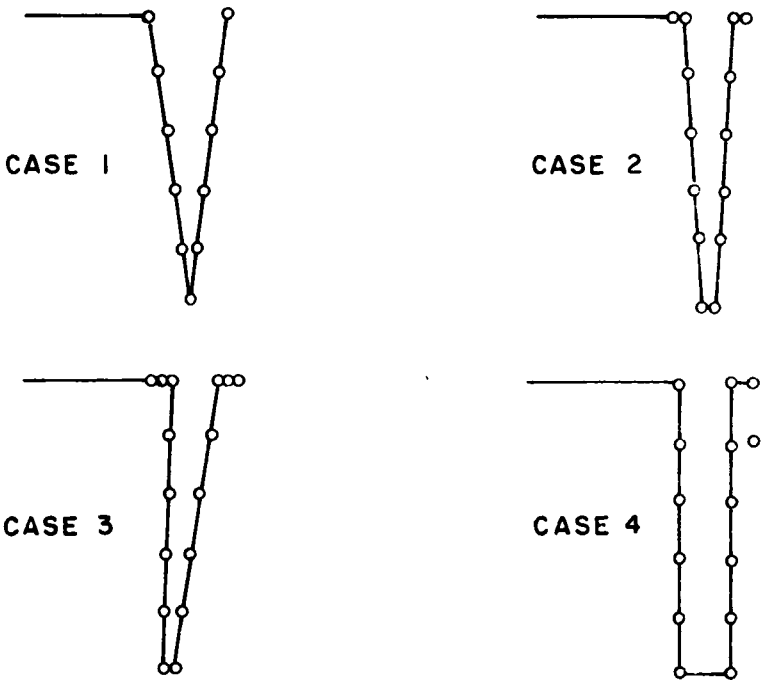


| CASE | X1 (cm) | N1 | X2 (cm) | N2 | X3 (cm) | N3 | X4 (cm) | N4 | X5 (cm) | N5 |
|---|---|---|---|---|---|---|---|---|---|---|
| 1 | 0.0 | 0 | 0.5 | 5 | 0.5 | 0 | 1.0 | 5 | 1.0 | 0 |
| 2 | 0.2 | 1 | 0.4 | 5 | 0.6 | 1 | 0.9 | 5 | 1.0 | 1 |
| 3 | 0.3 | 2 | 0.1 | 5 | 0.2 | 1 | 0.9 | 5 | 1.0 | 1 |
| 4 | 0.0 | 0 | 0.0 | 5 | 0.7 | 1 | 0.7 | 5 | 1.0 | 1 |

Fig. A3.

## SUBROUTINE GDPLDV

Subprogram GDPLDV is the groundplane surface division subroutine which is designed to symmetrically place 8 short segments around the source pair and divide the remaining segments along the rest of the groundplane. In use, this subprogram is called only once with the calling parameter NGP set to the number of matching segments one desires on the groundplane side of the origin. The 8 segments around the sources each have length equal to 0.25 x the distance between the sources. These segments are placed two to the left of the left source, four between the sources, and two to the right of the right source. The remaining NGP-8 segments are placed with at least one segment between the left endpoint and the symmetrically placed segments and the rest of the segments between the right of the symmetrically placed segments and the origin. The numbering of the endpoints is from the left endpoint and is indexed by variable MP. The cooridinate of the points are stored in [X(MP),H(MP)] and the surface normals and segment lengths in TN (MP) and SEGL(MP) respectively. These variables are shared with the main program and other subroutines through COMMON/MAINDV/. The subroutine listing follows.

```
      SUBROUTINE GDPLOV(NGP,MP)
      COMMON/MAINDV/ X(230),H(230),TN(230),SEGL(230),DEL,HC,G,EPL,EPR,WE
      COMMON /TAWIGD/ DZ1,DZ2
      DEL1=ABS(EPL/(NGP-4))
      DEL2=ABS((DZ2-DZ1)/2.0)
      X1=DZ2-DEL2
      X2=DZ2+DEL2
      X3=DZ1-DEL2
      X4=DZ1+DEL2
      WRITE(6,20) DEL1,DEL2,X1,X2,X3,X4
   20 FORMAT(6F12.6)
      TD=ABS(EPL-X1)
      N1=IFIX(TD/DEL1)
      IF(N1) 1,1,2
    2 DEL=TD/N1
      DO 3 I=1,N1
      X(I)=EPL+(I-1)*DEL
      SEGL(I)=DEL
    3 MP=I
      GO TO 4
    1 MP=1
      X(MP)=EPL
      SEGL(MP)=TD
    4 JJ=MP
      DEL=DEL2/2.0
      DO 5 I=1,8
      J=JJ+I
      X(J)=X1+(I-1)*DEL
      SEGL(J)=DEL
    5 MP=J
      JJ=MP
      N1=NGP-MP
      IF(N1) 6,6,7
    7 DEL=ABS(X4)/N1
      DO 9 I=1,N1
      J=JJ+I
      X(J)=X4+(I-1)*DEL
      SEGL(J)=DEL
    9 MP=J
    8 DO 10 I=1,MP
      TN(I)=1.57079
   10 H(I)=0.0
      RETURN
    6 WRITE(6,21)
   21 FORMAT(' POOR POINT SELECTION')
      GO TO 8
      END
```

## SUBROUTINE VSURDV

The subroutine VSURDV performs the surface division on arbitrary shape vee corrugations. Because of the periodicity of the corrugated surface, only one corrugation need be specified in detail and all the remaining corrugations are images. Figure A1 shows a period of the corrugated surface with the corner locations specified by the input parameters X1P to X5P. The input to this subroutine requires the corners be located in cm. rather than normalized to the corrugation period. Lines 28 to 32 of the main program remove this normalization. The segment endpoint numbering begins at "MP" at the origin and continues to the right endpoint. If the calling parameter KSURF is 1 (or 0) the surface will be closed (or open) and the numbering continued along the dotted path of Fig. A2 (or the numbering terminated). Some shapes which can be handled are shown in Fig. A3 and include the symmetric V-shape (case 1) and the square corrugation (case 4) as well as asymetric and flat bottom vee corrugations. The subroutine listing follows.

```
      SUBROUTINE VSURDV(X1,X2,X3,X4,TC,N1,N2,N3,N4,N5,MP,KSURF)
C IF KSURF=1, SURFACE IS CLOSED
C IF KSURF=0, SURFACE IS OPEN
      COMMON/MAINDV/ X(230),H(230),TN(230),SEGL(230),DEL,HC,G,EPL,EPR,WE
      DATA PI,PI2/3.1415926,1.5707963/
      M=MP
      JJ=MP
      IF(N1) 2,2,1
1     DEL=X1/N1
      DO 10 I=1,N1
      J=JJ+I
      X(J)=DEL*FLOAT(I-1)
      H(J)=0.
      TN(J)=PI2
      SEGL(J)=DEL
      MP=J
10    CONTINUE
2     XT=X(MP)+DEL
      DX=(X2-X1)/N2
      DH=HC/N2
      DEL=SQRT(DX*DX+DH*DH)
      T=ATAN2(DX,DH)
      JJ=MP
      DO 20 I=1,N2
      J=JJ+I
      X(J)=XT+DX*FLOAT(I-1)
      H(J)=-DH*FLOAT(I-1)
      TN(J)=T
      SEGL(J)=DEL
      MP=J
20    CONTINUE
      XT=X(MP)+DX
      JJ=MP
      IF(N3) 4,4,3
3     DEL=(X3-X2)/N3
      DO 30 I=1,N3
      J=JJ+I
      X(J)=XT+DEL*FLOAT(I-1)
      H(J)=-HC
      TN(J)=PI2
      SEGL(J)=DEL
      MP=J
30    CONTINUE
```

```
      XT=X(MP)+DEL
4     DX=(X4-X3)/N4
      DH=HC/N4
      DEL=SQRT(DX*DX+DH*DH)
      T=1.57079+ATAN2(DH,DX)
      JJ=MP
      DO 40 I=1,N4
      J=JJ+I
      X(J)=XT+DX*FLOAT(I-1)
      H(J)=-HC+DH*FLOAT(I-1)
      TN(J)=T
      SEGL(J)=DEL
      MP=J
40    CONTINUE
      XT=X(MP)+DX
      JJ=MP
      IF(N5) 6,6,5
5     DEL=(TC-X4)/N5
      DO 50 I=1,N5
      J=JJ+I
      X(J)=XT+DEL*FLOAT(I-1)
      H(J)=0.0
      TN(J)=PI2
      SEGL(J)=DEL
      MP=J
50    CONTINUE
6     NTCELL=IFIX((EPR+0.1)/TC)
      NCELL=N1+N2+N3+N4+N5
      DO 60 N=2,NTCELL
      JJ=M+NCELL*(N-1)
      DO 61 I=1,NCELL
      J=JJ+I
      K=M+I
      X(J)=X(K)+TC*(N-1)
      H(J)=H(K)
      TN(J)=TN(K)
      SEGL(J)=SEGL(K)
61    MP=J
60    CONTINUE
      IF(KSURF) 7,7,8
7     MP=MP+1
      X(MP)=NTCELL*TC
      H(MP)=0.0
      WRITE(6,62)
62    FORMAT(/' OPEN SURFACE'/)
      RETURN
8     XMAX=NTCELL*TC
      JJ=MP
      JJ=MP
      HP=HC+0.1
      N=IFIX(HP*8./WE)
      DEL=HP/N
      DO 70 I=1,N
      J=JJ+I
      X(J)=XMAX
      H(J)=-(I-1)*DEL
      TN(J)=0.0
      SEGL(J)=DEL
70    MP=J
      JJ=MP
      K=IFIX((XMAX-EPL)*8./WE)
      DEL=(XMAX-EPL)/K
      DO 80 I=1,K
      J=JJ+I
      X(J)=XMAX-(I-1)*DEL
      H(J)=-HP
      TN(J)=-PI2
```

```
      SEGL(J)=DEL
   80 MP=J
      DO 90 I=1,N
      JJ=MP
      EPL=AMAX1(HP*(1./WF)
      DEL=HP/N
      DO 90 I=1,N
      J=JJ+I
      X(J)=EPL
      H(J)=-HP+(I-1)*DEL
      TN(J)=PI
      SEGL(J)=DEL
   90 MP=J
      MP=MP+1
      X(MP)=EPL
      H(MP)=0.0
      TN(MP)=0.0
      SEGL(MP)=0.0
      WRITE(6,91)
   91 FORMAT(/' CLOSED SURFACE'/)
      RETURN
      END
```

## SUBROUTINE CO

Subroutine CO generates the coupling coefficients for the "$\gamma$" matrix of section II. The subroutine finds the magnetic field at segment "MR" due to a current on segment "MC" by performing a 5-point Gaussian integration along the length of segement "MC". The program listing follows.

```
      COMPLEX FUNCTION CO(MR,MC)
C     THIS GIVES THE OLD MATRIX COEFFICIENTS
      COMMON/MAINDV/ X(230),H(230),TN(230),SEGL(230),DEL,HC,G,EPL,EPR,WE
      COMPLEX DJC
      COMMON /COG/ DJC
      COMPLEX AHAN21
      DATA GU1,GU2,GU3,GU4,GU5,GW1,GW2,GW3,GW4,GW5/-0.9061798,-0.5384693
     2,0.00,0.5384693,0.9061798,0.2369268,0.4786287,0.568888,0.4786287,
     3 0.2369268/
      IF(MR.NE.MC) GO TO 100
      CO=CMPLX(0.500,0.0)
      GO TO 200
  100 CONTINUE
      DEL=SEGL(MC)
      DEL2=DEL/2.
      XMM=0.500*(X(MR)+X(MR+1))
      HXMM=0.50*(H(MR)+H(MR+1))
      EPL=X(MC)
      EPU=X(MC+1)
      DVDEP=(EPU-EPL)/2.0
      DVSMEP=(EPU+EPL)/2.0
      XU5=GU5*DVDEP+DVSMEP
      XU1=GU1*DVDEP+DVSMEP
      XU2=GU2*DVDEP+DVSMEP
      XU3=GU3*DVDEP+DVSMEP
      XU4=GU4*DVDEP+DVSMEP
      HU=H(MC+1)
      HL=H(MC)
      DELH=(HU-HL)/2.
      DHM=(HU+HL)/2.0
      HXU1=GU1*DELH+DHM
      HXU2=GU2*DELH+DHM
      HXU3=GU3*DELH+DHM
      HXU4=GU4*DELH+DHM
      HXU5=GU5*DELH+DHM
      THN=TN(MC)
      XR=XMM-XU1
      YR=HXMM-HXU1
      R1DN=(XR*COS(THN)+YR*SIN(THN))/SQRT(XR*XR+YR*YR)
      XR=XMM-XU2
      YR=HXMM-HXU2
      R2DN=(XR*COS(THN)+YR*SIN(THN))/SQRT(XR*XR+YR*YR)
      XR=XMM-XU3
      YR=HXMM-HXU3
      R3DN=(XR*COS(THN)+YR*SIN(THN))/SQRT(XR*XR+YR*YR)
      XR=XMM-XU4
      YR=HXMM-HXU4
      R4DN=(XR*COS(THN)+YR*SIN(THN))/SQRT(XR*XR+YR*YR)
      XR=XMM-XU5
      YR=HXMM-HXU5
      R5DN=(XR*COS(THN)+YR*SIN(THN))/SQRT(XR*XR+YR*YR)
      FACTOR=SQRT(DVDEP*DVDEP+DELH*DELH)
      CO=FACTOR*(
     2+(GW1*AHAN21(G*SQRT(((XU1-XMM)**2)+((HXU1-HXMM)**2)))*R1DN )
     2+(GW2*AHAN21(G*SQRT(((XU2-XMM)**2)+((HXU2-HXMM)**2))) *R2DN)
```

```
      2+(GW3*AHAN21(G*SQRT(((XU3-XMM)**2)+((HXU3-HXMM)**2))) *R3DN)
      2+(GW4*AHAN21(G*SQRT(((XU4-XMM)**2)+((HXU4-HXMM)**2))) *R4DN)
      2+(GW5*AHAN21(G*SQRT(((XU5-XMM)**2)+((HXU5-HXMM)**2))) *R5DN))
       C0=C0*OJC
200   CONTINUE
      RETURN
      END
```

## SUBROUTINE AHAN21

Subroutine AHAN21 is a double precision Hankel function of type 2 and order 1. The function is generated using the polynomial approximations for $J_1(X)$ and $Y_1(X)$ presented in Abramowitz[13]. The program listing follows.

```
      FUNCTION AHAN21(X)
C     THIS IS THE HANKEL FUNCTION OF TYPE 2 AND OF ORDER 1
      DOUBLE PRECISION XD,DX,A1,A2,A3,A4,A5,A6,HJ1,B1,B2,B3,B4,B5,AHJ1,
     2TDX,A1,A2,A3,A4,A5,A6,T1,T2,T3,T4,T5,T6,T7,DSQX,B6
      COMPLEX AHAN21
      DX=DBLE(X)
      IF (X.GT.3.0) GO TO 200
      XD=DX*DX/9.0D+00
      A1=-0.3176ID-03+0.1109D-04*XD
      A2=0.00443319D+00+A1*XD
      A3=-0.03954289D+00+A2*XD
      A4=0.21093573D+00+A3*XD
      A5=-0.56249985D+00+A4*XD
      A6=0.5D+00+A5*XD
      HJ1=A6*DX
      B1=-0.0400976D+00+0.0027873D+00*XD
      B2=0.3123951D+00+B1*XD
      B3=-1.3164827D+00+B2*XD
      B4=2.1682709D+00+B3*XD
      B5=0.2212091D+00+B4*XD
      B6=-0.6366198D+00+B5*XD
      AHJ1=(B6/DX)+HJ1*DLOG(DX/2.0)*0.63661977
      AHAN21=CMPLX(SNGL(HJ1),-SNGL(AHJ1))
      GO TO 300
  200 TDX=3.0/DX
      A1=0.00113653D+00-0.00020033*TDX
      A2=-0.00249511D+00+A1*TDX
      A3=.00017105D+00+A2*TDX
      A4=0.01659667D+00+A3*TDX
      A5=0.1560-05+A4*TDX
      A6=0.79788456D+00+A5*TDX
      T1=0.00079824D+00-0.00029166D+00*TDX
      T2=0.00074348D+00+T1*TDX
      T3=-0.00637879D+00+T2*TDX
      T4=0.00005650D+00+T3*TDX
      T5=0.12499612D+00+T4*TDX
      T6=-2.35619449D+00+T5*TDX
      T7=DX+T6
      DSQX=A6/DSQRT(DX)
      AHAN21=CMPLX(SNGL(DSQX*DCOS(T7)),-SNGL(DSQX*DSIN(T7)))
  300 CONTINUE
      RETURN
      END
```

## SUBROUTINE CROUTN

The nonsymmetric matrix inversion subroutine solves a system of simultaneous linear equations with complex coefficients using the method developed by P.D. Crout[10]. The set of equations are related to the calling parameters shown in the following listing by

$$[C]\,[X] = [F]$$

where [C] is the array of complex coupling coefficients
[X] is the column vector of length N of unknowns,
[F] is the column vector of length N of known variables before inversion; after inversion, the array contains the solution vector.
NDIM is the dimension of [C] and [F] in the subroutines; NDIM $\geq$ N.

```
      SUBROUTINE CROUTN(C,F,N,NDIM)
      COMPLEX C(NDIM,NDIM),F(NDIM),S
C     NONSYMMETRIC CROUT
C     FIRST COLUMN OK
C     TO GET THE FIRST ROW
      DO 10 J=2,N
 10   C(1,J)=C(1,J)/C(1,1)
C          NOW WORK ON ROW AND COLUMN SET K
      DO 11 K=2,N
      KMO=K-1
      KPO=K+1
C      TO GET DIAGONAL ELEMENT
      S=CMPLX(0.0,0.0)
      DO 12 IK=1,KMO
 12   S=S+C(K,IK)*C(IK,K)
      C(K,K)=C(K,K)-S
C            TO GET ELEMENTS IN COLUMN  K BELOW ROW K
      IF (KPO.GT.N) GO TO 17
      DO 13 IROW=KPO,N
      S=CMPLX(0.0,0.0)
      DO 14 JJ=1,KMO
 14   S=S+C(IROW,JJ)*C(JJ,K)
 13   C(IROW,K)=C(IROW,K)-S
C          TO GET ELEMENTS IN ROW K TO THE RIGHT OF COLUMN K
      DO 15 ICOL=KPO,N
      S=CMPLX(0.0,0.0)
      DO 16 JR=1,KMO
 16   S=S+C(K,JR)*C(JR,ICOL)
 15   C(K,ICOL)=(C(K,ICOL)-S)/C(K,K)
 17   CONTINUE
 11   CONTINUE
C     THIS ENDS THE MATRIX FACTORIZATION
C     THIS BEGINS THE BACK SUBSTUTION
C     CONVERSION OF SOURCE SIDE
      F(1)=F(1)/C(1,1)
      DO 90 IJ=2,N
      S=CMPLX(0.0,0.0)
      IJMO=IJ-1
      DO 91 IK=1,IJMO
 91   S=S+C(IJ,IK)*F(IK)
 90   F(IJ)=(F(IJ)-S)/C(IJ,IJ)
C          NOW FOR FINAL BACK SUBSTITITION
      NMO=N-1
      DO 160 L=1,NMO
      K=N-L
      KPO=K+1
      S=CMPLX(0.0,0.0)
      DO 175 JO=KPO,N
 175  S=S+C(K,JO)*F(JO)
 160  F(K)=F(K)-S
C     THIS ENDS THE BACK SUBSTITUTIONS
      RETURN
      END
```

## SUBROUTINE WILLUM

Subroutine WILLUM is the subprogram used to generate the incident fields at RHO, PHI from a magnetic line source pair located at DZ1 and DZ2. The line source amplitudes are $1/Z_0$ and phased to produce a cardiod pattern directed along $\theta = 0$ (toward the corrugations). The Fortran listing follows.

```
      SUBROUTINE WILLUM(RHO,PHI,HINC,WE)
      COMMON /MAVIGD/ DZ1,DZ2
C THIS SUBROUTINE CALCULATES THE NEAR FIELDS AT RHO,PHI RADIATED BY A PAIR
C WIRES SEPARATED BY D AND H ABOVE ORIGIN WITH MAGNETIC CURRENTS FK1 AND FK
      COMPLEX HINC,FK1,FK2,JN(2,6),J
      COMPLEX ARG
      PI=3.14159
      DEGR=PI/180.
      FK=2.*PI/WE
      FK1=(1.,0.)
      J=(0.,1.)
      FK2=J
      H=0.
      DZ1=-4.
      DZ2=-6.
      RHO1=SQRT(DZ1*DZ1+H*H)
      RHO2=SQRT(DZ2*DZ2+H*H)
      PH1=ATAN2(H,DZ1)
      PH2=ATAN2(H,DZ2)
      RHO1P=SQRT(ABS(RHO*RHO+RHO1*RHO1-2.*RHO*RHO1*COS(PH1-PHI*DEGR)))
      RHO2P=SQRT(ABS(RHO*RHO+RHO2*RHO2-2.*RHO*RHO2*COS(PH2-PHI*DEGR)))
      ARG=CMPLX(FK*RHO1P,0.)
      IF (CABS(ARG).GE.0.01) GO TO 1
      HINC=FK1
      GO TO 2
    1 CALL BESSEL(ARG,JN)
      HINC=FK1*JN(1,5)
    2 CONTINUE
      ARG=CMPLX(FK*RHO2P,0.)
      IF (CABS(ARG).GE.0.01) GO TO 3
      HINC=FK2
      GO TO 4
    3 CALL BESSEL(ARG,JN)
      HINC=HINC+FK2*JN(1,5)
    4 CONTINUE
C Z0=377. SCALE FACTOR REMOVED
      HINC=HINC*FK/4.
      RETURN
      END
```

## SUBROUTINE BESSEL

BESSEL generates $J_0(x)$, $N_0(x)$, $J_1(x)$, $N_1(x)$, $H_0^{(2)}(x)$, $H_1^{(2)}(x)$ and their derivatives using a power series for small complex arguments, $|Z| \leq 12$, and the asymptotic forms for $|Z| > 12$. These variables are stored in array JN and returned as a calling parameter. The Fortran listing follows.

```
      SUBROUTINE BESSEL(Z,JN)
      COMPLEX JN(2,6),Z,TERMJ,TERMN,MZ24,T1,T2,T3
C JN(1,1)=J0(Z)
C JN(2,1)=J1(Z)
C JN(1,2)=N0(Z)
C JN(2,2)=N1(Z)
C JN(1,3)=D/DX(J0(X))
C JN(2,3)=D/DX(J1(X))
C JN(1,4)=D/DX(N0(X))
C JN(2,4)=D/DX(N1(X))
C JN(1,5)=H0(2)(X)
C JN(2,5)=H1(2)(X)
C JN(1,6)=D/DX(H0(2)(X))
C JN(2,6)=D/DX(H1(2)(X))
      PI=3.14159
      IF(CABS( Z ).GE.12.0) GO TO10
      FACTOR=0.0
      TERMN=(0.,0.)
      MZ24=-0.25*Z*Z
      TERMJ=(1.0,0.0)
      DO 1 NP=1,2
      N=NP-1
      JN(NP,1)=TERMJ
      M=0
    2 M=M+1
      TERMJ=TERMJ*MZ24/FLOAT(M*(N+M))
      JN(NP,1)=JN(NP,1)+TERMJ
      IF(NP.NE.1) GO TO 3
      FACTOR=FACTOR+1.0/FLOAT(M)
      TERMN=TERMN+TERMJ*FACTOR
    3 ERROR=CABS(TERMJ)
      IF(ERROR.GT.1.0E-10) GO TO 2
    1 TERMJ=0.5*Z
      JN(1,2)=(2.0/3.1415927)*((0.5772157+CLOG(0.5*Z))*JN(1,1)-TERMN)
   11 CONTINUE
      JN(2,2)=(JN(2,1)*JN(1,2)-2.0/(3.1415927*Z))/JN(1,1)
      JN(1,3)=-JN(2,1)
      JN(2,3)=JN(1,1)-JN(2,1)/Z
      JN(1,4)=-JN(2,2)
      JN(2,4)=JN(1,2)-JN(2,2)/Z
      JN(1,5)=JN(1,1)-(0.0,1.0)*JN(1,2)
      JN(2,5)=JN(2,1)-(0.0,1.0)*JN(2,2)
      JN(1,6)=JN(1,3)-(0.0,1.0)*JN(1,4)
      JN(2,6)=JN(2,3)-(0.0,1.0)*JN(2,4)
      RETURN
C ASYMPTOTIC FORMS USED FOR ARGUMENTS GREATER THAN 12.
   10 T1= Z -CMPLX(PI/4.,0.)
      T2= Z -CMPLX(3.*PI/4.,0.)
      T3=CSQRT(2./(PI* Z ))
      JN(1,1)=T3*CCOS(T1)
      JN(2,1)=T3*CCOS(T2)
      JN(1,2)=T3*CSIN(T1)
      JN(2,2)=T3*CSIN(T2)
      GO TO 11
      END
```

## SUBROUTINE PLOT

PLOT is a line printer plotting subroutine which plots up to 10 different curves (stored in the Y array) on the same set of coordinates. The value "X" is plotted along the page while the "Y" array is plotted between YMIN and YMAX across a line on the page with Y(1) plotted as a "*", Y(2) plotted as ".", etc. A call with "IND" = 0 places the Y scale across the page and for IND equal to a multiple of 10, places tic marks across the page. The PLOT subroutine must be called in a "DO" loop to plot an array of data. The Fortran listing follows.

```
      SUBROUTINE PLOT( X,Y,N,IND,YMAX,YMIN)
      DIMENSION M(119),YLABEL(6),Y(10),MARK(10)
      DATA MARK(1),MARK(2),MARK(3),MARK(5),MARK(6),MARK(7),MARK(8),
     2MARK(9),MARK(10),MARK(4)/1H*,1H.,1HI,1HO,1HN,1HH,1H1,1HZ,1H-,1HX/
      DATA IBLANK,NOPT,IPLUS/1H ,1H',1H+/
      IF(IND)1,1,11
    1 WRITE(6,3)
    3 FORMAT(1H1//25X,48HORDER IN WHICH PLOT SYMBOLS ARE USED  *,IXONH1Z
     *-//30X,39HTHE SYMBOL ($) INDICATES OFF-SCALE DATA//)
      DO7J=9,119
    7 M(J)=MARK(10)
      NCOUNT=10
      SCALE=100.0/(YMAX-YMIN)
      LLL=(-YMIN*SCALE)+11.5
      DO8J=1,6
      R=J-1
    8 YLABEL(J)=R*20.0/SCALE+YMIN
      WRITE(6,9) (YLABEL(I),I=1,6)
    9 FORMAT(6X,1PE9.2,5(1PE20.2) /  )
      GOTO132
   11 NCOUNT=NCOUNT+1
      DO99J=1,119
   99 M(J)=IBLANK
      IF(LLL.GE.11.AND.LLL.LE.110)M(LLL)=MARK(10)
      IF(NCOUNT-10)133,132,133
  132  DO89J=11,111,20
   89  M(J)=IPLUS
  133 DO20J=1,N
      L=(Y(J)-YMIN)*SCALE+0.5
      IF(L)14,17,17
   14 IF(L+10)15,16,16
   15 M(1)=NOPT
      GOTO20
   16   LL=L+11
        M(LL)=MARK(J)
      GOTO20
   17 IF(L-108)18,19,19
   18  LL=L+11
       M(LL)=MARK(J)
      GOTO20
   19 M(119)=NOPT
   20 CONTINUE
      IF(NCOUNT-10)21,25,21
   21 WRITE(6,24) (M(J ), J=1,119)
   24 FORMAT(1X,119A1)
      GOTO27
   25 WRITE(6,26) (X,(M(J),J=9,119))
   26 FORMAT(1X,F8.3  ,111A1)
      NCOUNT=0
   27  CONTINUE
      RETURN
      END
```

## APPENDIX B

## HIGHER ORDER MODES IN A SQUARE CORRUGATION

Because of the limited number of matching points available, only four segments were used on each of the vertical walls of each of the corrugations. Over the range of corrugation depths considered, this meant that 8 to 16 matching points per wavelength were used. While this density is adequate to represent the TEM mode in the square corrugation, any appreciable amplitude higher order mode would either not be observed or could introduce errors in the computations. Thus it was necessary to verify that any higher order modes were of small amplitude and only over a limited portion of the corrugation. To do this, the closed surface of Fig. B1 was used with the computer program of Appendix A. The model included a single corrugation illuminated by a magnetic line source located $0.5\lambda$ (4 cm) from the corrugation.

The 30 segments per vertical wall in the corrugation yields 60 to 240 matching points per wavelength over the range of depths considered ($0.125 \leq d/\lambda < 0.5$). The relative surface current which exists at each point on the surface of the corrugation is shown on the plots in Fig. B2a to B2d for corrugation depths of $0.125\lambda$, $0.25\lambda$, $0.375\lambda$ and $0.499\lambda$ respectively. On these plots, the surface current amplitude, normalized to the $1/Z_0$ amplitude magnetic line source, is plotted along the corrugation wall where the current is flowing. The amplitude function $\cos 2\pi(d-H)/\lambda$ corresponding to that of the TEM mode whose maximum is set equal to the maximum current computed in the corrugation is also shown. Notice that in each case the calculated current (the series of steps) very nearly fits the cosinusoidal distribution anticipated for the TEM mode in the corrugation. Also, the computed currents on the two walls at the same depth differ only slightly. Thus the higher order modes are of low amplitude amd only over a small region of the corrugation. The loss associated with higher order modes is negligible.

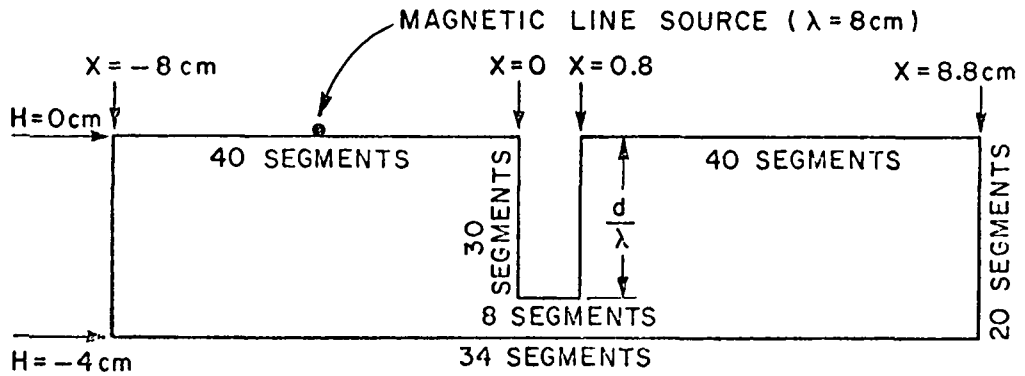


Fig. B1. Surface model used to study higher order modes in a single square corrugation.

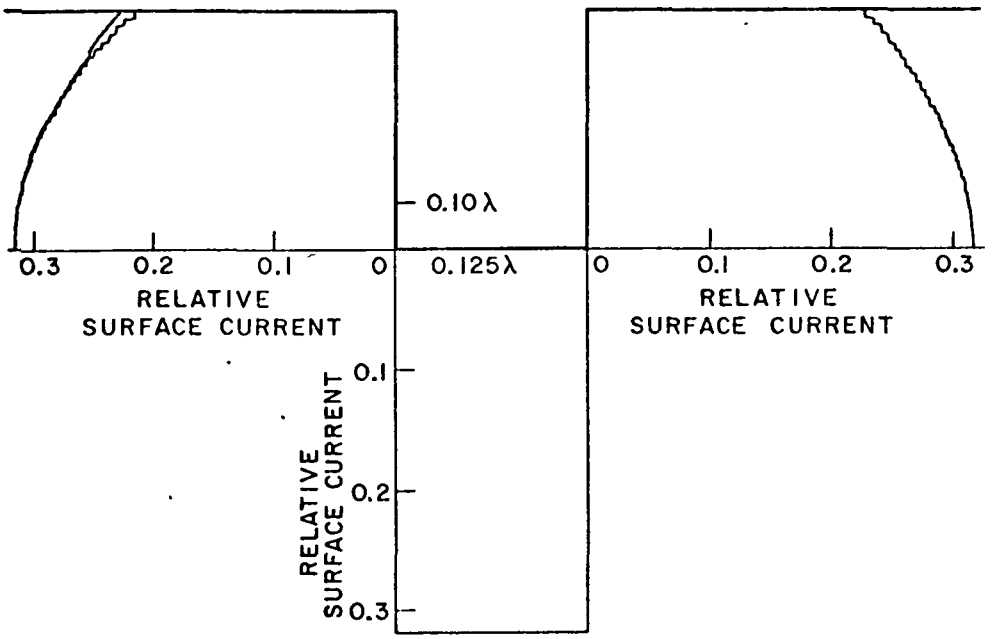


Fig. B2a. Relative surface current existing on the walls of a square corrugation at a corrugation depth of $d/\lambda = 0.125$.

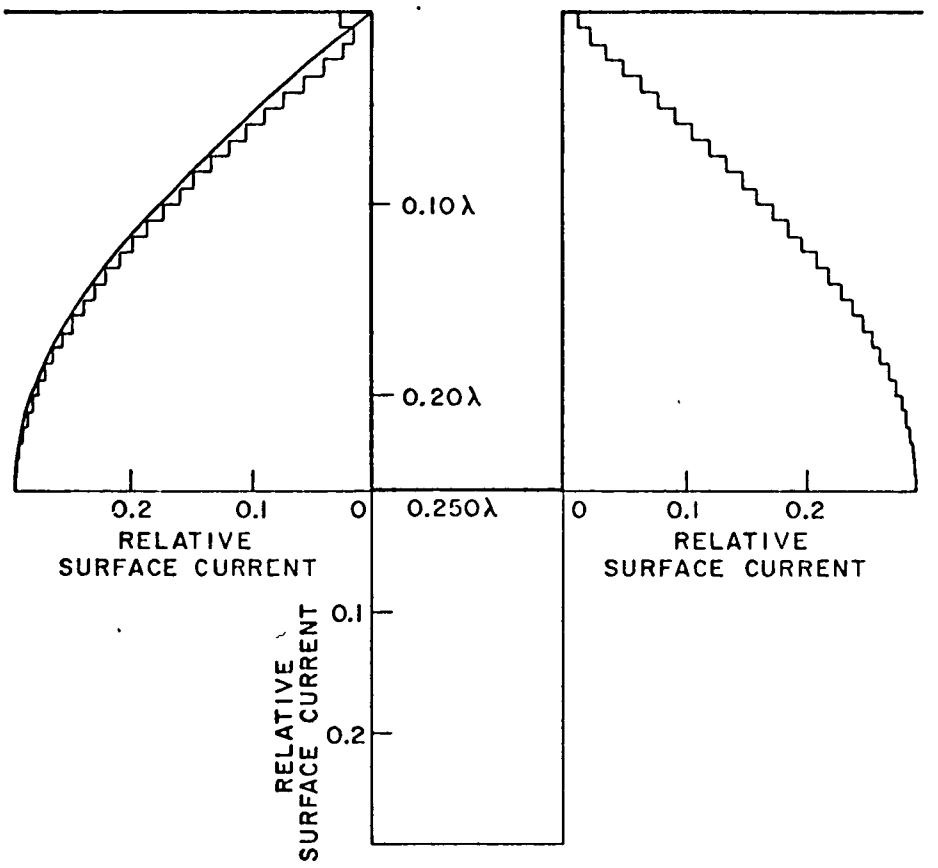


Fig. B2b. Relative surface current existing on the walls of a square corrugation at a corrugation depth of $d/\lambda = 0.250$.

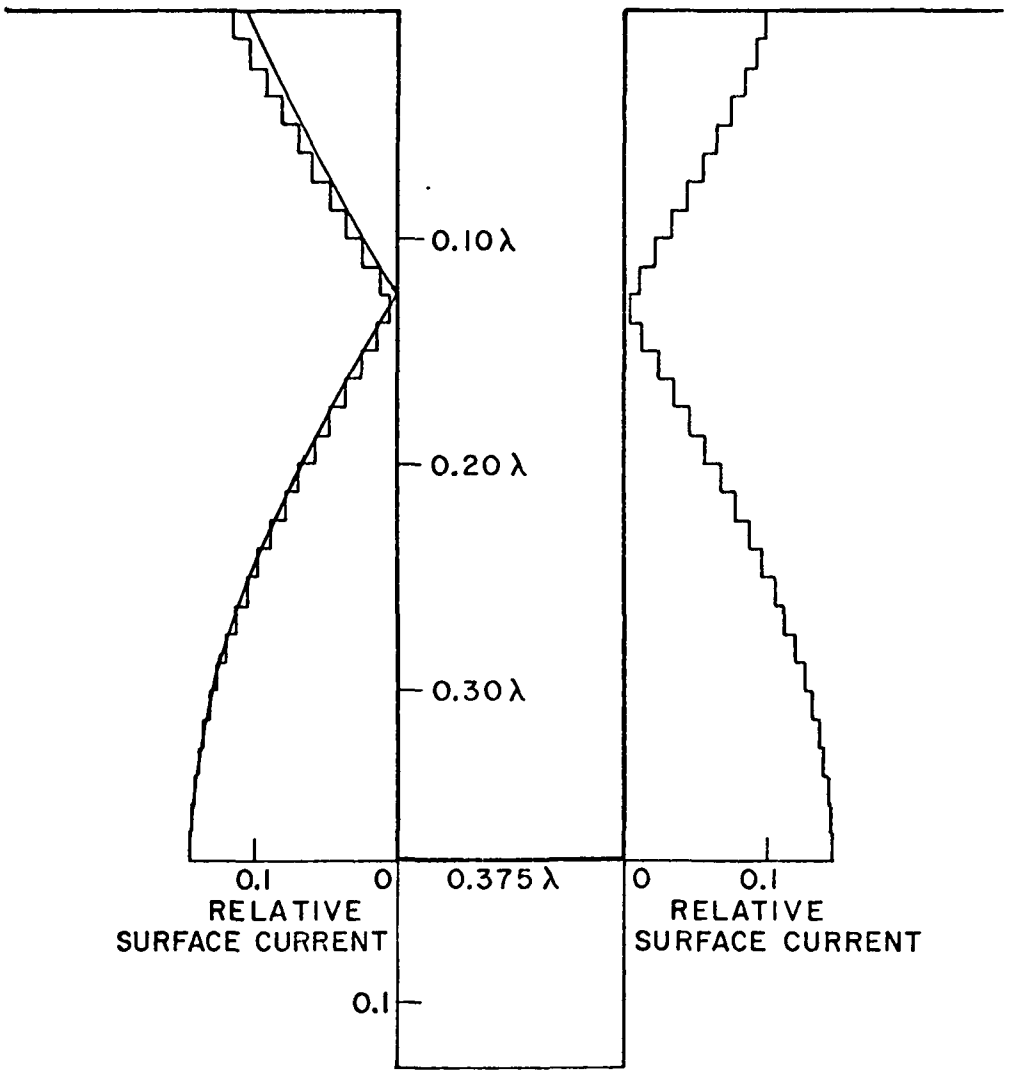


Fig. B2c. Relative surface current existing on the walls of a square corrugation at a corrugation depth of $d/\lambda = 0.375$.

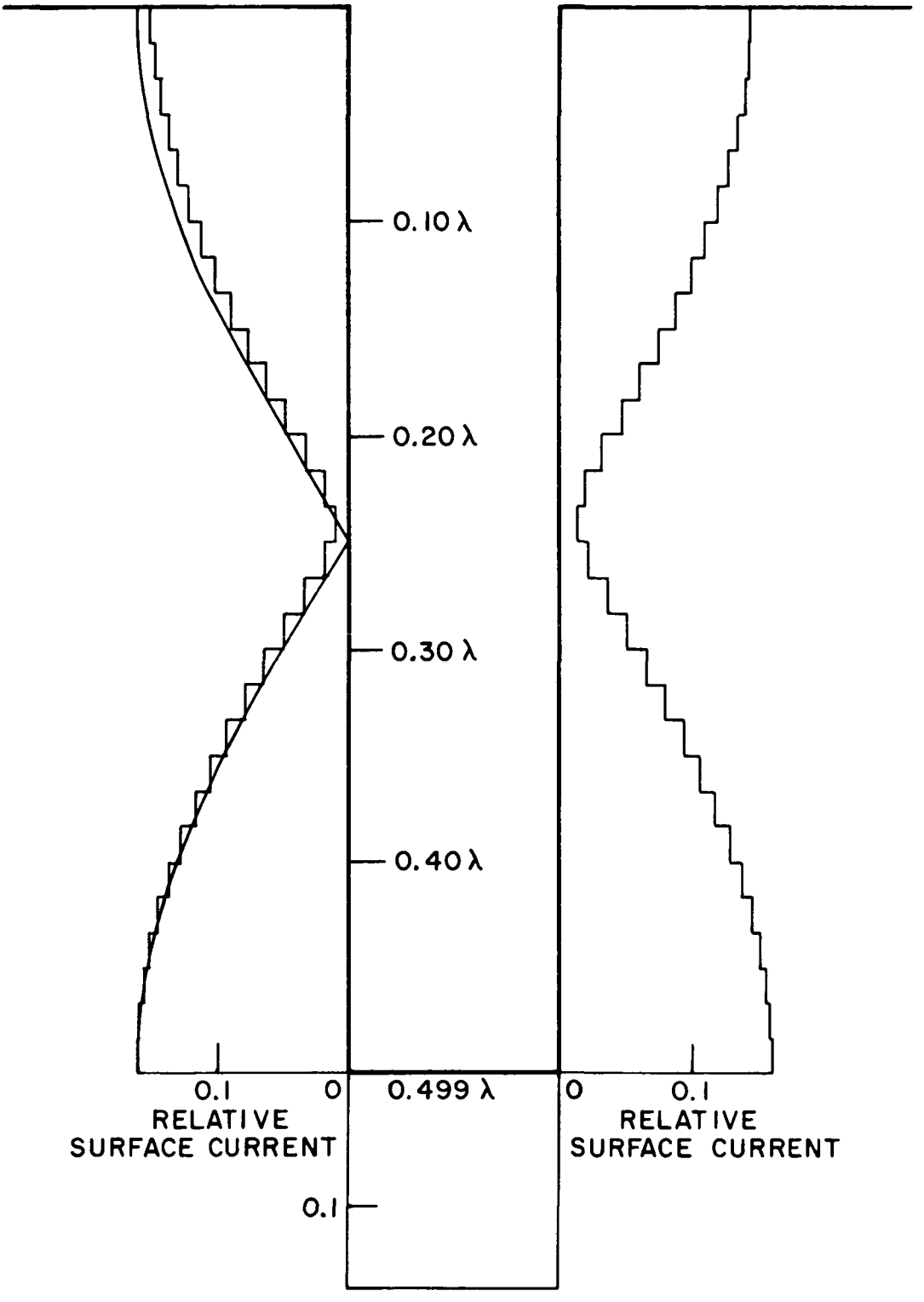


Fig. B2d. Relative surface current existing on the walls of a square corrugation at a corrugation depth of $d/\lambda = 0.499$.

## REFERENCES


1. Caldecott, R., Mentzer, C.A., Peters, L., Jr. and Toth, J., "High Performance S-Band Horn Antennas for Radiometer Use," The Ohio State University ElectroScience Laboratory, Columbus, Ohio, NASA Contractor Report CR-2133, January 1973.

2. Lawrie, R. and Peters, L., Jr., "Modification of Horn Antennas for Low Sidelobe Levels," IEEE Transactions on Antennas and Propagation, September 1966, Vol. AP-14, No. 5.

3. Caldecott, R., Mentzer, C. and Peters, L., Jr., "Properties of Corrugated Horns," 1971 USNC-URSI Spring Meeting, Washington, D.C.

4. Bahret, W.E. and Peters, L., Jr., "Small Aperture Small-Flare Angle Corrugated Horns," Communication in IEEE Transactions an Antennas and Propagation, July 1968, Vol. AP-16, No. 4.

5. Mentzer, C.A. and Peters, L., Jr., "Excitation of 'Forbidden Zone' Corrugations for Corrugated Horn Applications," 1972 IEEE/G-AP Symposium, Williamsburg, Virginia.

6. Buchmeyer, S.K., "Corrugations Lock Horns with Poor Beamshapes," Microwaves, Vol. 12, No. 1, January 1973, pp.44-49.

7. Minnet, H.C. and Thomas, B. Mac A., "A Method of Synthesizing Radiation Patterns with Axial Symmetry," IEEE Trans. on Antennas and Propagation, September, 1966.

8. Rumsey, V.H., "Horn Antennas with Uniform Power Patterns Around their Axis," IEEE Trans. on Antennas and Propagation, September 1966.

9. Harrington, R.F., Field Computation by Moment Methods, The Macmillian Company, New York, 1968, pp. 50-55.

10. Westlake, J., A Handbook of Numerical Matrix Inversion and Solution of Linear Equations, Wiley, 1968, pp. 10-14.

11. Russo, P.M., Rudduck, R.C., and Peters, L., Jr., "A Method for Computing E-Plane Patterns of Horn Antennas," IEEE Trans. on Antennas and Propagation, Vol. AP-13, No. 2, March 1965, pp.219-224.

12. Harrington, R.F., Time Harmonic Electromagnetic Fields, The McGraw-Hill Book Company, New York, 1961, pp. 208-213.

13. Abramowitz, M. and Stegun, I.A., Handbook of Mathematical Functions, U.S. Department of Commerce, National Bureau of Standards Applied Mathematics Series, U.S. Government Printing Office, 1966, p. 370.

NATIONAL AERONAUTICS AND SPACE ADMINISTRATION
WASHINGTON, D.C. 20546

OFFICIAL BUSINESS
PENALTY FOR PRIVATE USE $300

SPECIAL FOURTH-CLASS RATE
BOOK

POSTAGE AND FEES PAID
NATIONAL AERONAUTICS AND
SPACE ADMINISTRATION
451

U.S.MAIL

POSTMASTER: If Undeliverable (Section 158 Postal Manual) Do Not Return

*"The aeronautical and space activities of the United States shall be conducted so as to contribute . . . to the expansion of human knowledge of phenomena in the atmosphere and space. The Administration shall provide for the widest practicable and appropriate dissemination of information concerning its activities and the results thereof."*

—NATIONAL AERONAUTICS AND SPACE ACT OF 1958

# NASA SCIENTIFIC AND TECHNICAL PUBLICATIONS

TECHNICAL REPORTS: Scientific and technical information considered important, complete, and a lasting contribution to existing knowledge.

TECHNICAL NOTES: Information less broad in scope but nevertheless of importance as a contribution to existing knowledge.

TECHNICAL MEMORANDUMS: Information receiving limited distribution because of preliminary data, security classification, or other reasons. Also includes conference proceedings with either limited or unlimited distribution.

CONTRACTOR REPORTS: Scientific and technical information generated under a NASA contract or grant and considered an important contribution to existing knowledge.

TECHNICAL TRANSLATIONS: Information published in a foreign language considered to merit NASA distribution in English.

SPECIAL PUBLICATIONS: Information derived from or of value to NASA activities. Publications include final reports of major projects, monographs, data compilations, handbooks, sourcebooks, and special bibliographies.

TECHNOLOGY UTILIZATION PUBLICATIONS: Information on technology used by NASA that may be of particular interest in commercial and other non-aerospace applications. Publications include Tech Briefs, Technology Utilization Reports and Technology Surveys.

***Details on the availability of these publications may be obtained from:***

**SCIENTIFIC AND TECHNICAL INFORMATION OFFICE**

**NATIONAL AERONAUTICS AND SPACE ADMINISTRATION**

**Washington, D.C. 20546**